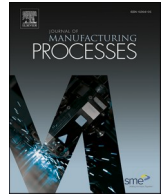




Contents lists available at ScienceDirect

Journal of Manufacturing Processes

journal homepage: www.elsevier.com/locate/manpro

Engineering surface topography analysis using an extended discrete modal decomposition

Yiping Shao^a, Fengcong Xu^a, Jun Chen^a, Jiansha Lu^{a,*}, Shichang Du^b

^a College of Mechanical Engineering, Zhejiang University of Technology, Hangzhou 310023, China

^b School of Mechanical Engineering, Shanghai Jiao Tong University, No. 800 Dongchuan Road, Shanghai 200240, China

ARTICLE INFO

Keywords:

Surface topography
Filtering
Discrete modal decomposition
Engineering surface

ABSTRACT

Surface topography is a crucial link to connect precision manufacturing processes and product performance. Discrete modal decomposition (DMD) is recently developed filtering method for surface topography analysis, which projects the engineering surface onto a series of modal basis. Comparing with traditional filtering methods, DMD method is well applied to various engineering surfaces with holes effectively without end effect. However, each decomposed mode of DMD has not been mapped to the surface components, which lacks physical dimensions. Hence, a novel extended discrete modal decomposition (EDMD) is proposed to achieve the multi-scale engineering surface topography analysis in this paper. The proposed EDMD method including data transforming, surface inverse modeling, extended discrete modal decomposition and quantitative evaluation. Gaussian filter, robust Gaussian regression filter, spline filter and extended tetrolet transform are used as comparisons of the proposed method in numerical simulations. The EDMD method perform well both in continuous and discontinuous engineering surfaces, which overcomes the border distortion especially for discontinuous engineering surfaces and complements the physical dimension of each decomposed mode. Three real engineering surface case studies illustrate the proposed EDMD method is effective and applicable.

1. Introduction

Engineering surface topography has a significant influence to parts, whether that affects the functional behaviors, processing costs or working life of parts [1]. Meanwhile, surface topography can be influenced by many factors during the precision manufacturing processes, such as chatter, tool wear, cutting force and vibration [2–6]. Surface topography is commonly composed by multi-scale components, which is distinguished by various wavelengths or frequencies. According to the difference of the wavelength, engineering surface is generally separated to three components. Primary form is the long wavelength component, while roughness is the short wavelength component. The wavelength of waviness is between the primary form and roughness. Different surface components have different origins and association with various part functional properties, such as wear and sealing [7–10]. Moreover, each surface component plays a crucial role to engineering part and it is meaningful to investigate the filtering technology of engineering surface.

Surface filtering technology is referred to that the different scale

surface components are separated from the measured engineering surface for further analysis. Many classical and advanced filtering methods are reviewed in [11,12]. As the current ISO standard filtering method, Gaussian filter [13] is well applied to all kinds of continuous surfaces except the well-known end effect. End effect is a distortion of the border values that occurs in most of filtering methods due to the disappearance of the boundary data. With the serious end effect of Gaussian filter, many modifications of Gaussian filtering have been proposed. Binkman et al. [14,15] proposed a Gaussian regression filtering method which combines the regular Gaussian filter with polynomial fit to reduce end effect. Seewing [16] proposed a Linear and robust gaussian regression filter method using the weight iteration function to enhance the robustness. Janecski [17] proposed recursive Gaussian filters to eliminate the end effects. Whitehouse [18] extended the current Gaussian filters using Hermite polynomials to enhance scratch and flaw detection. Kondo [19] proposed a L2-norm Gaussian filter, which indicated a high robustness, high-speed processing and compatibility. Besides the modifications of Gaussian filters, other advanced filtering methods were investigated to reduce the end effect. Krystek et al. [20,21] proposed a

* Corresponding author.

E-mail addresses: syp123gh@zjut.edu.cn (Y. Shao), 2112002328@zjut.edu.cn (F. Xu), 2112102402@zjut.edu.cn (J. Chen), ljs@zjut.edu.cn (J. Lu), lovbin@sjtu.edu.cn (S. Du).

<https://doi.org/10.1016/j.jmapro.2023.02.005>

Received 22 June 2022; Received in revised form 15 January 2023; Accepted 3 February 2023

Available online 20 February 2023

1526-6125/© 2023 The Society of Manufacturing Engineers. Published by Elsevier Ltd. All rights reserved.

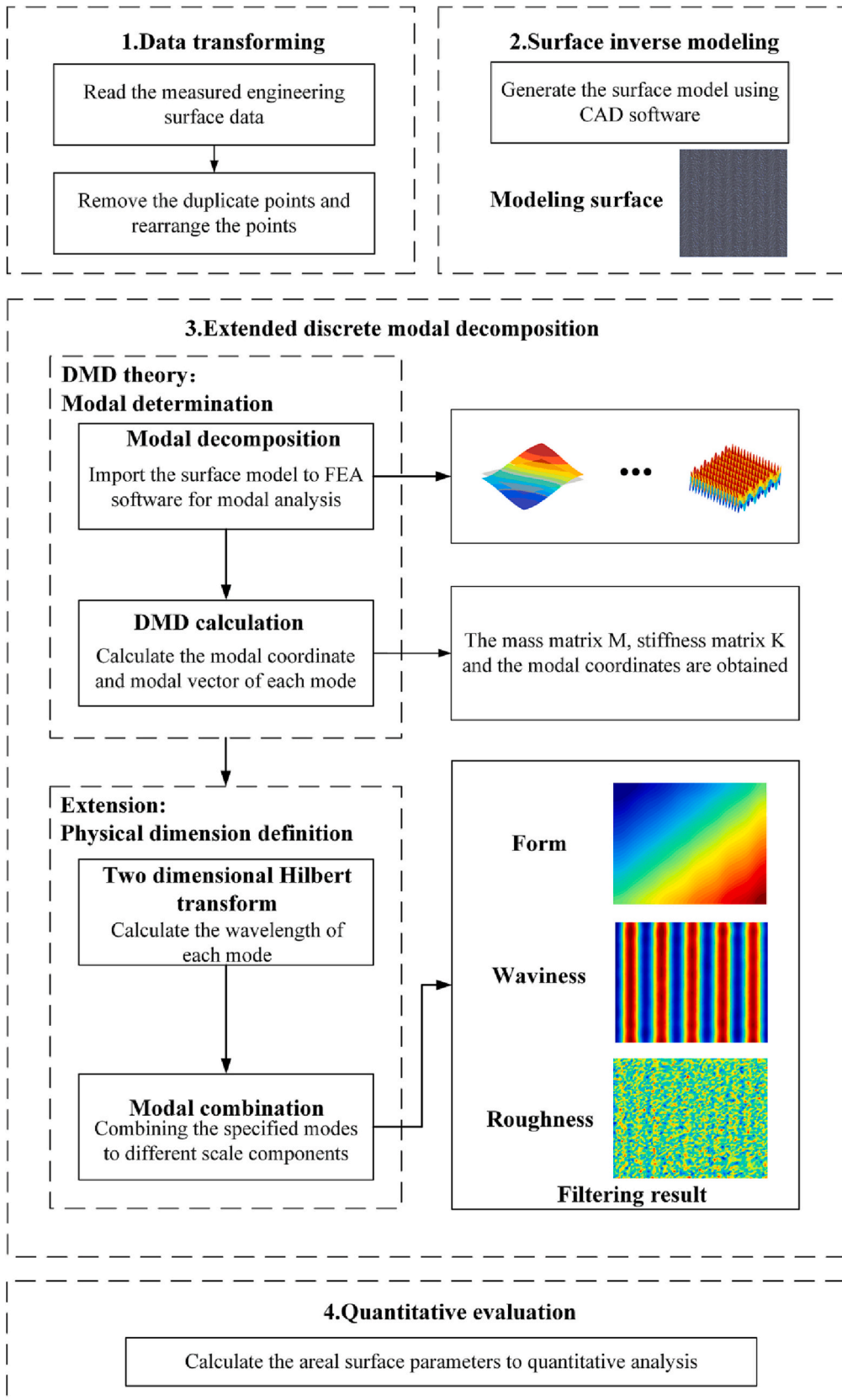


Fig. 1. The structural frame of the proposed EDMD method.

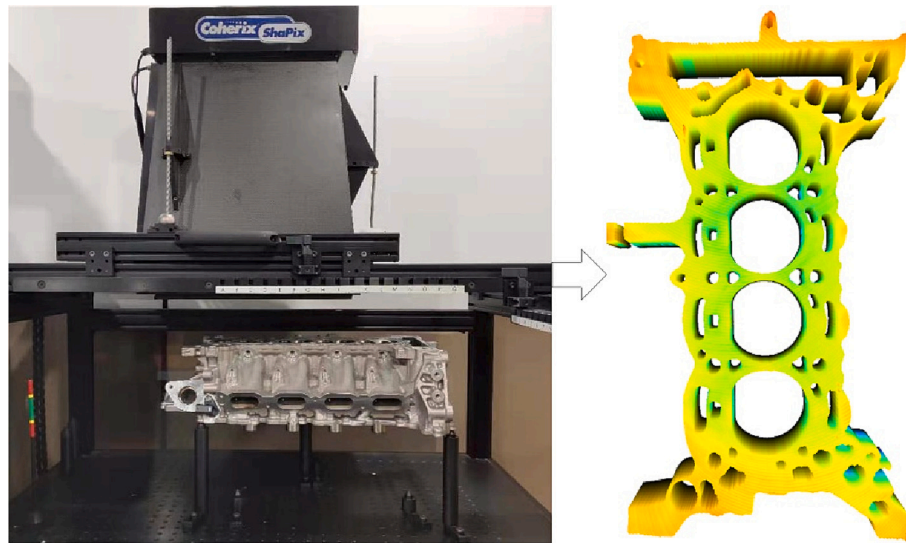


Fig. 2. The noncontact laser holographic interferometry measuring instrument.

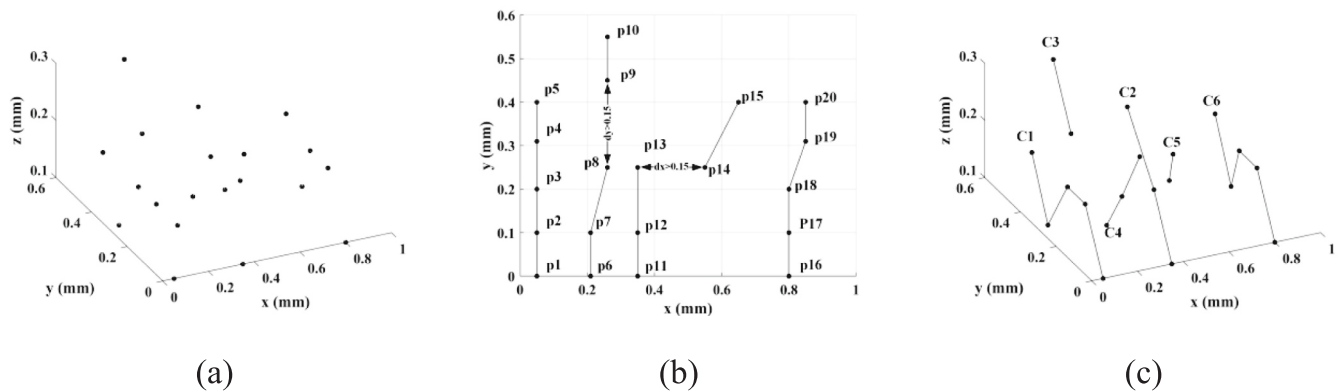


Fig. 3. Example of points rearrangement (a) the point set M (b) the point set M1 expressed in two-dimensional coordinates (c) the rearranged curves.



Fig. 4. Example of inverse modeling (a) the rearranged file (b) the generated surface.

spline filter which is well used as a form filter and can reduce the end effect. Jiang et al. [22] developed a lifting wavelet representation approach based on biorthogonal wavelet which overcome the phase distortion. Fu et al. [23] separated the components of real engineering surface using wavelet transform and verified its feasibility. Huang et al. [24] decomposed complicated data into small of intrinsic mode functions (IMF) to achieve empirical mode decomposition (EMD) filtering method. Du et al. [25,26] based on high definition metrology successively proposed a shearlet-based method and a modified bi-dimensional empirical mode decomposition method to analyze the workpiece engineering surface topography. Shao et al. [27,28] developed an extended

bi-dimensional empirical wavelet transform and extended tetrolet transform for engineering surfaces filtering to reduce the end effect. Jiang et al. [29,30] proposed and applied a morphological filtering method based on alpha shape, which runs fast and enable applied to freeform surface and non-uniformly sampled surfaces. Lou et al. [31] achieved freeform surface topography analysis using watershed segmentation method. Most of the methods mentioned above overcome or reduce the end effect for the continuous surface without holes. However, these methods fail when dealing with the discontinuous surface with holes and the end effect reappears. With tighter tolerance and higher performance standards, it appears a variety of key engineering surfaces contains one or more holes, such as cylinder block and head, pump housing, valve body and so on. It is necessary to explore a well-worked filtering method both for continuous surfaces and discontinuous surfaces with holes.

More recently, a new filtering method named discrete modal decomposition (DMD) has been proposed [32–34], which is the nonlinear and non-stationary filtering method based on the Eigen basis originated from structural dynamic problem. In this method, the engineering surface is decomposed into a series of discrete functions called modes. Then, the surface components are combined by the specific modes with different wavelengths or frequencies. The method can well decompose the all kinds of surface theoretically, such as continuous surface, discontinuous surface or even freeform surface. However, each decomposed mode of DMD method has not been linked to the surface

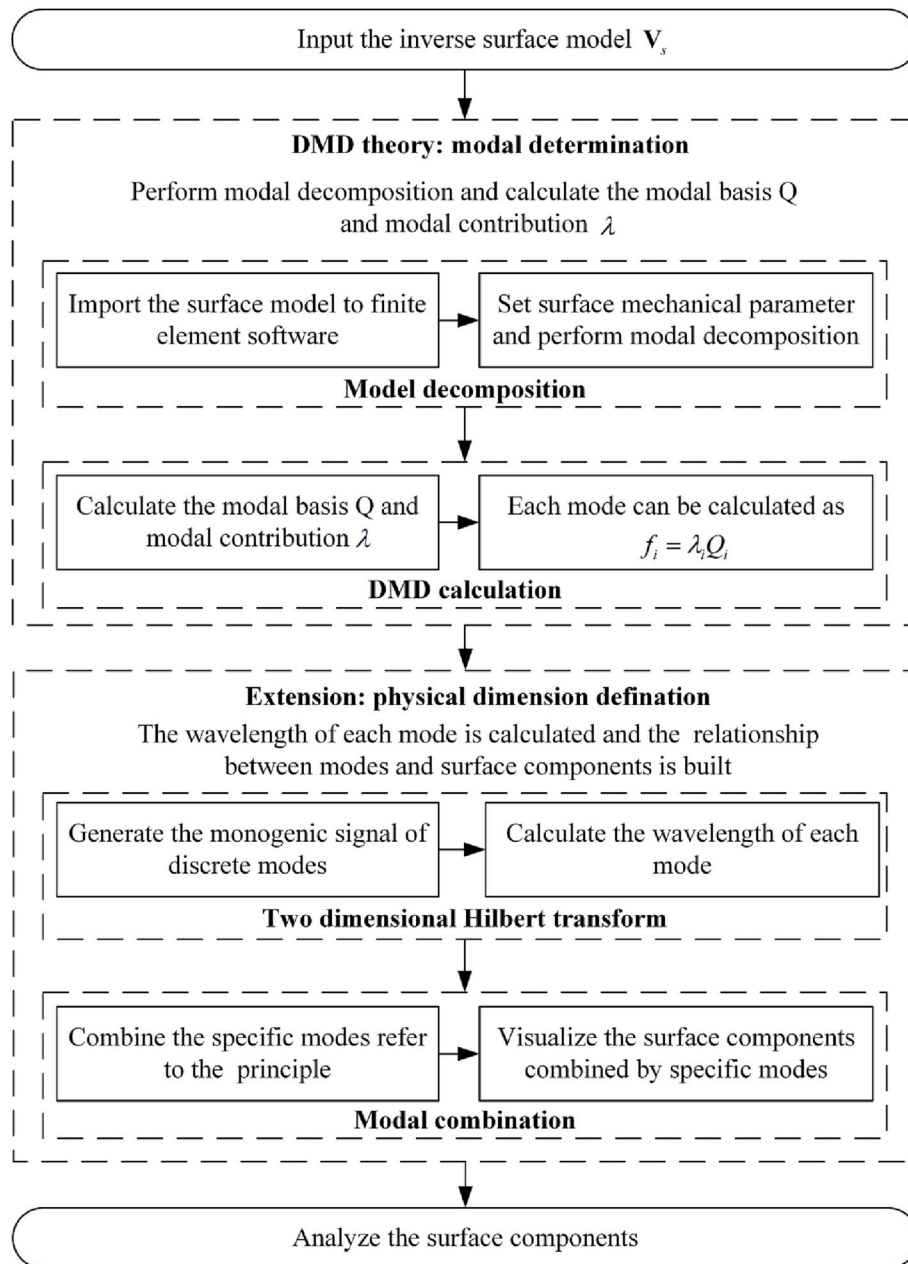


Fig. 5. The EDMD process.

components. In order to identify the physical dimensions of these discrete modes, the original DMD method needs to be improved. Hence, the main contribution of this paper is that an extended discrete modal decomposition (EDMD) based filtering method is proposed to analyze the engineering surface topography. The EDMD method can perform well both in continuous and discontinuous engineering surfaces, which overcomes the border distortion especially for discontinuous engineering surfaces. Furthermore, it complements the physical dimension of each mode and builds the corresponding relationship between discrete modes and surface components.

The rest paper is structured as follows: Section 2 presents the fundamental of discrete modal decomposition theory. Section 3 describes the detail of the proposed EDMD surface filtering method. Section 4 shows two numerical simulation cases to explore the feasibility of the proposed method. Section 5 presents three real engineering surface case studies to validate the application of the proposed method. Finally, Section 6 draws the conclusions and discusses the further research.

2. Fundamental of DMD method

Discrete modal decomposition (DMD) is based on the modal shape of structural mechanics which is proposed by Samper [32]. Similar to empirical modal decomposition (EMD) [35], the basic idea of DMD is to decompose a signal within a spectral basis built from Eigen modes. For each Eigen mode, the spectral basis is also named Eigen basis or modal basis, which is defined by its eigenvectors or modal vectors. The DMD method can be roughly divided into three modules including inherent modal solution, boundary condition determination and modal vector projection.

Module 1: inherent modal solution

The measured surface V_m is projected into different modal basis by solving a dynamic structural problem in the linear dynamics, and the modal basis is derived from the resolution of a classical dynamic

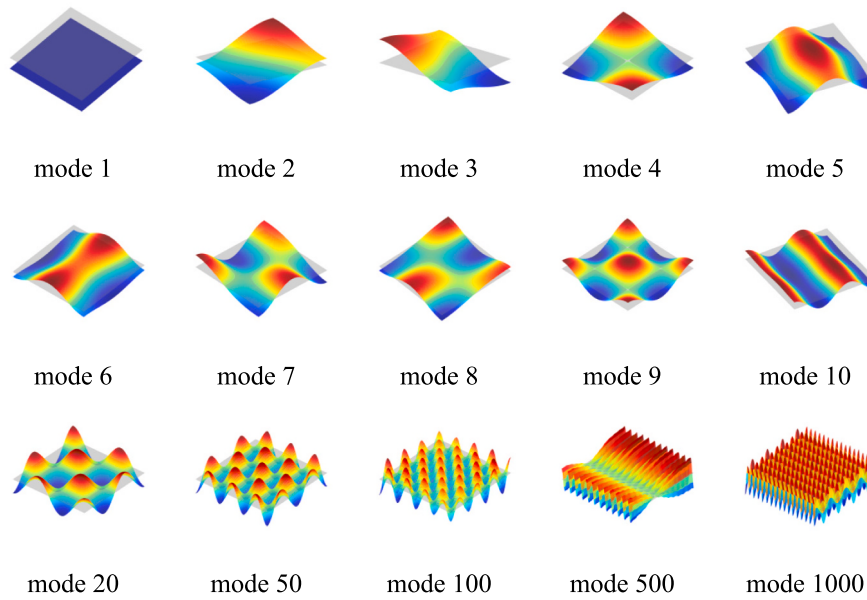


Fig. 6. Modal basis Q of a square surface.

Table 1
The combination principle.

The wavelength of mode	Combination principle
$\lambda_j \geq \lambda_f (j > 0)$	$\sum_{i=0}^j f_i(x, y)$ represents form component
$\lambda_{j+1}, \lambda_{j+2}, \dots, \lambda_k \in [\lambda_c, \lambda_j] (j < k < N)$	$\sum_{i=j+1}^k f_i(x, y)$ represents waviness component
$\lambda_{k+1}, \lambda_{k+2}, \dots, \lambda_m \in [\lambda_s, \lambda_c] (m < N)$	$\sum_{i=k+1}^m f_i(x, y)$ represents roughness component
$\lambda_{m+1} \leq \lambda_s$	$\sum_{i=m+1}^N f_i(x, y)$ represents micro-burrs
$\lambda_0 < \lambda_f$	Errors occurred in analysis

equation:

$$M\ddot{q} + Kq = 0 \tag{1}$$

where **M** and **K** are the mass matrix and stiffness matrix with the size of $N \times N$, respectively. q is the displacement vector with the size of $N \times 1$, which is used to describe the modal shape and defined as:

Table 2
The calculating equations of areal surface parameters.

	Parameter name	Calculation formula ^a
Height parameters	Arithmetical mean height S_a	$S_a = \frac{1}{A} \iint_A z(x, y) dx dy$
	Root mean square height S_q	$S_q = \sqrt{\frac{1}{A} \iint_A z^2(x, y) dx dy}$
	Maximum height S_z	$S_z = S_p + S_v$
	Skewness S_{sk}	$S_{sk} = \frac{1}{S_q^3} \left[\frac{1}{A} \iint_A z^3(x, y) dx dy \right]$
	Kurtosis S_{ku}	$S_{ku} = \frac{1}{S_q^4} \left[\frac{1}{A} \iint_A z^4(x, y) dx dy \right]$
Hybrid parameters	Root mean square of the surface gradient S_{dq}	$S_{dq} = \sqrt{\frac{1}{A} \iint_A \left[\left(\frac{\partial z(x, y)}{\partial x} \right)^2 + \left(\frac{\partial z(x, y)}{\partial y} \right)^2 \right] dx dy}$
	Area ratio S_{dr}	$S_{dr} = \frac{1}{A} \left[\frac{1}{A} \iint_A \left(\sqrt{1 + \left(\frac{\partial z(x, y)}{\partial x} \right)^2 + \left(\frac{\partial z(x, y)}{\partial y} \right)^2} - 1 \right) dx dy \right]$
Functional parameters	Core height S_k	Distance between the highest and lowest level of the core surface

^a $A = \iint_A dx dy$ is the evaluation area, $z(x, y)$ denotes the height value of coordinate x and y in two dimensional coordinates. S_p and S_v are the maximum peak height and the maximum pit height within A , respectively.

$$q_i(t) = Q_i \cos(\omega_i t) \tag{2}$$

where Q_i denotes the modal vector or modal basis of the mode i , ω_i denotes the corresponding natural pulsation, and the number of i is controlled by the number of nodes and their degrees of freedom (DOF). Combining Eqs. (1) and (2), ω_i and model vector space Q can be calculated by the following equation:

$$(K - \omega_i^2 M)Q = 0 \tag{3}$$

Module 2: boundary condition determination

Boundary condition is the necessary and sufficient condition to obtain the solution of modal vector. In generally, free boundary and fixed boundary are the two main categories of boundary conditions, which will lead to different forms of modes including free mode, local fixed mode and full fixed mode. Once the displacement in certain directions is collinear with the feature, the displacement of this direction



Fig. 7. The inverse model (a) continuous simulated model (b) discontinuous simulated model.

cannot be generated and the corresponding coefficient is set to zero.

Module 3: modal vector projection

The measured surface V_m project into the modal basis Q can be written as:

$$\left((Q^T * Q)^{-1} * Q^T \right) V_m = \lambda \tag{4}$$

where Q denotes the modal basis and composed by each mode vector Q_i , λ denotes modal coordinates, which composed by each mode’s contribution or modal coefficient λ_i .

As the modal vector Q_i contains all the possible forms of the ideal signal, the measured surface V_m is projected into each modal vector,

which can be expressed as the sum of the linear combination of the modal vector Q_i and the residual ϵ (see Eq. (4)).

$$V_m = \{f_1, f_2, f_3, \dots, f_N\} = \sum_{i=1}^N \lambda_i Q_i + \epsilon \tag{5}$$

where λ_i denotes the modal coefficient of the mode i and N denotes the number of decomposed mode. Based on the above equations, the discrete solution of the modal vector Q_i and the modal coefficient λ_i can be computed by Finite Element Analysis (FEA) when the boundary condition is determined. Meanwhile, the decomposed subsurface can be represented by the corresponding modal vector Q_i . Therefore, the DMD method can be concluded as following steps:

- Step 1: Input a measured surface V_m ;
- Step 2: Set the boundary condition and material properties;
- Step 3: Perform modal decomposition;
- Step 4: Export and calculate the modal basis Q and modal coefficient λ_i ;
- Step 5: Decomposed the input signal V_m into various sub signal f_i .

3. The proposed method

3.1. Overview of the proposed method

This section introduces the proposed engineering surface analysis method named extended discrete modal decomposition (EDMD). It contains four steps which are data transforming, surface inverse

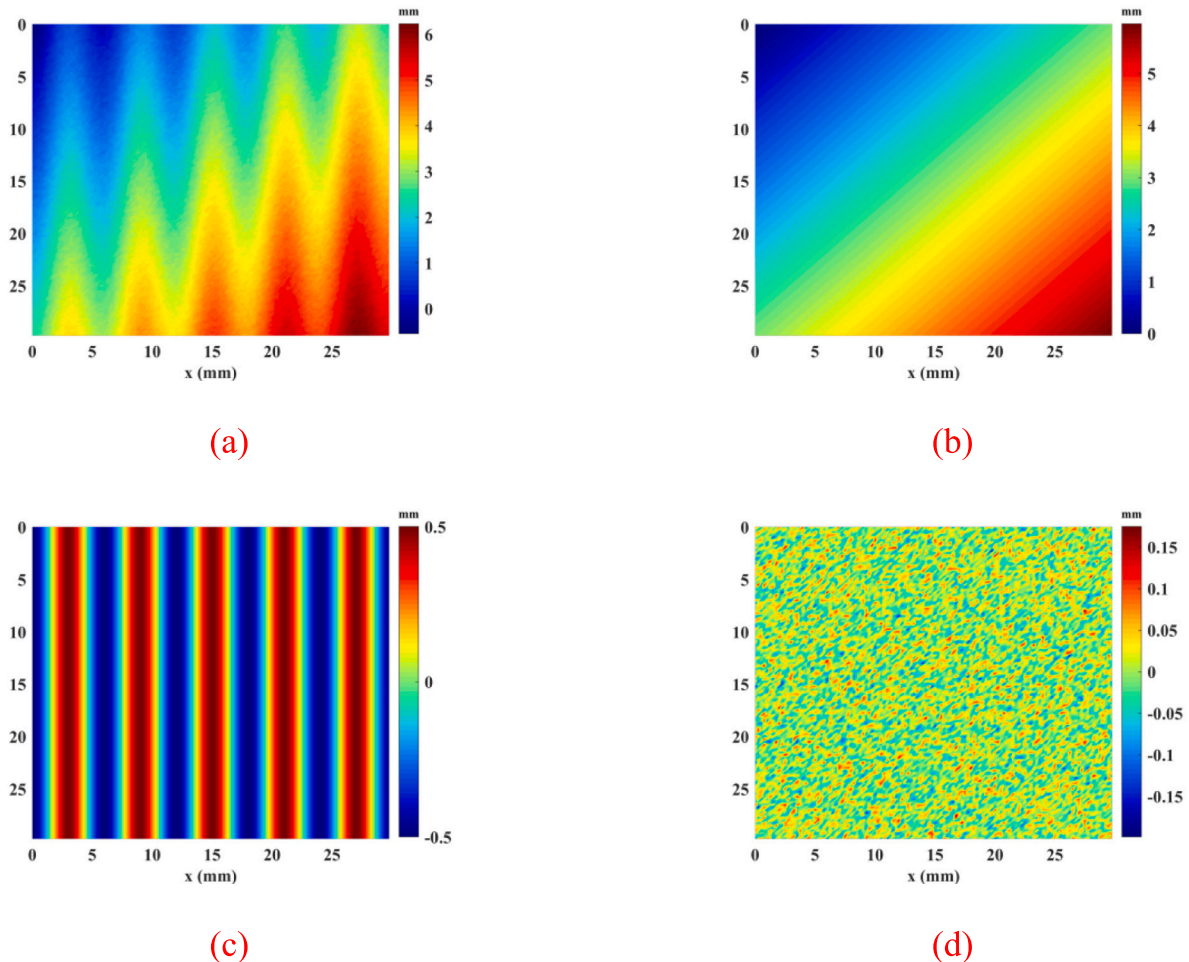


Fig. 8. All components of the continuous simulated surface (a) the original simulated surface (b) form component (c) waviness component (d) roughness component.

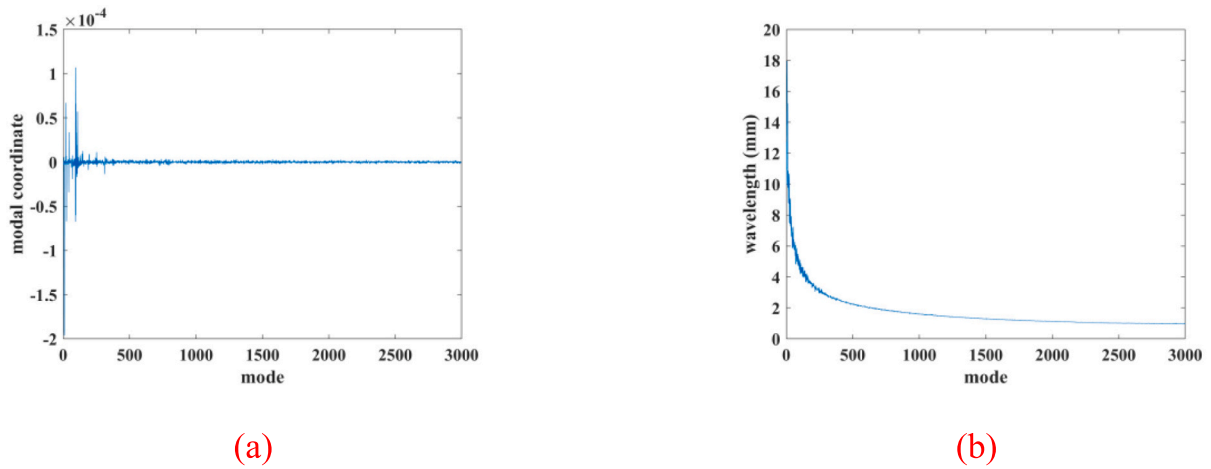


Fig. 9. The modal coordinates and the wavelengths (a) modal coordinates of the first 3000 modes (b) the wavelengths of the first 3000 modes.

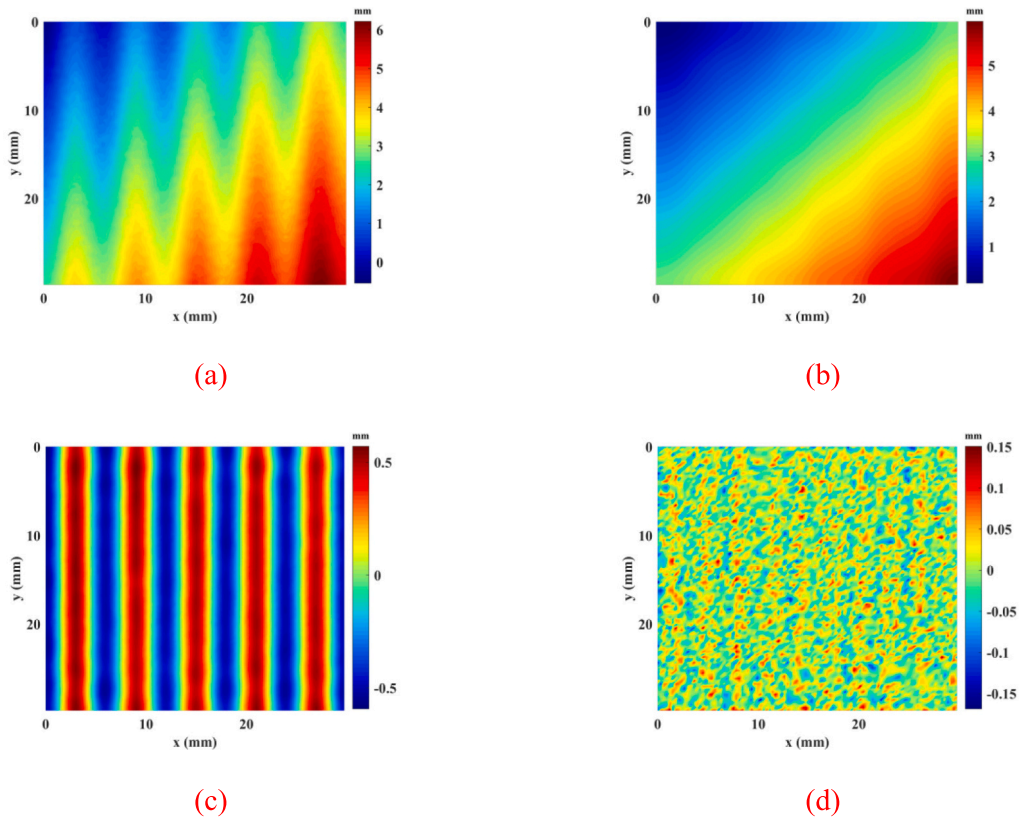


Fig. 10. The filtering results of EDMD method (a) the reconstructed surface (b) form component (c) waviness component (d) roughness component.

modeling, extended discrete modal decomposition and quantitative evaluation. The structural frame of the proposed EDMD method is described as Fig. 1, and the method can be summarized as follows:

- Step 1: Data transforming. Read the measured surface data points, then the duplicate and outlier points are removed. The rest data points are rearranged based on the coordinates of points and the rearranged file are generated.
- Step 2: Surface inverse modeling. Import the rearranged file to the CAD software and generate the surface model by inverse modeling.
- Step 3: Extended discrete modal decomposition. The EDMD analysis is divided to four modules: modal decomposition, DMD calculation, two dimensional Hilbert transform and modal combination. The

processes of modal decomposition and DMD calculation are the original DMD method, which achieves modal determination. Two dimensional Hilbert transform and modal combination are the extension, which achieves physical dimension definition. Using finite element analysis to perform modal decomposition and obtain the mass matrix M and the stiffness matrix K for DMD calculation, thereby the modal contributions λ and modal basis Q are calculated. The wavelength of each discrete mode is calculated by two dimensional Hilbert transform. Combining the specified modes which accord with the principle of modal combination, and different scale components are visualized.

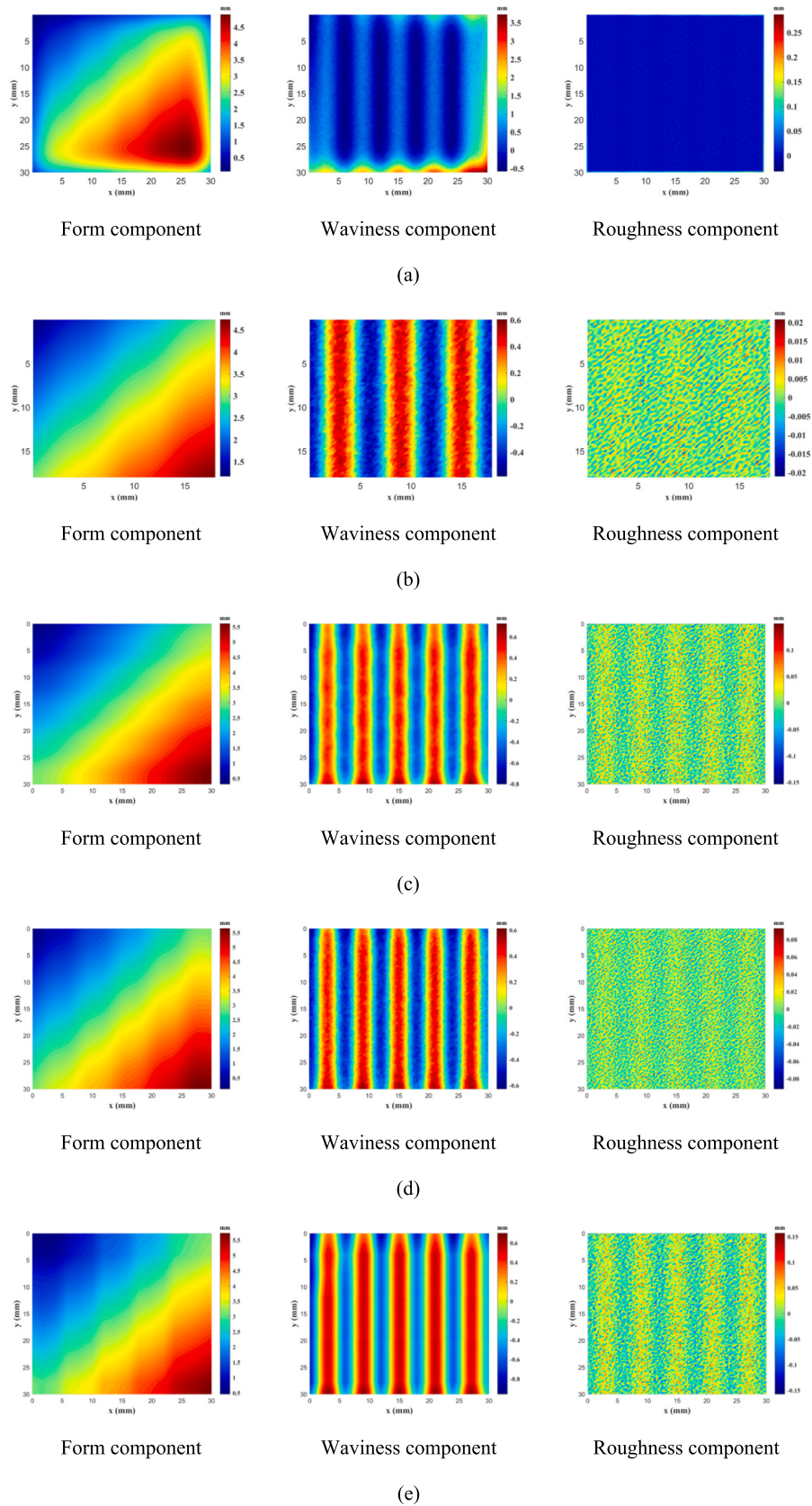


Fig. 11. The filtering results (a) Gaussian filter (b) Cutoff Gaussian filter (c) robust Gaussian regression filter (d) spline filter (e) extended tetrolet transform.

Table 3

The evaluation of the waviness components.

Unit (mm)	S_q	S_{sk}	S_{ku}	S_z	S_p	S_v	S_a	S_{dq}	S_{dr}	S_k
Simulated	0.3510	0.4775	1.7088	1.0000	0.6036	0.3964	0.3118	0.3467	0.0096	0.4283 ^a
CG	0.3475	0.4691	1.6626	0.9681	0.6030	0.3651	0.2848	0.3484	0.0097	0.4061
RGR	0.3415	0.4596	1.7015	1.0510	0.6301	0.4209	0.3033	0.3412	0.0095	0.4606
Spline	0.3238	0.4861	1.7353	1.0408	0.6109	0.4299	0.2884	0.3205	0.0088	0.4033
ETT	0.3831	0.4328	1.6632	1.0921	0.6571	0.435	0.3383	0.3745	0.0091	0.4523
EDMD	0.3335	0.4678	1.8162	1.0571	0.6370	0.4201	0.2948	0.3593	0.0089	0.4077
D_1	-1.00 %	-1.76 %	-2.70 %	-3.19 %	-0.10 %	-7.90 %	-8.66 %	0.49 %	1.04 %	-5.18 %
D_2	-2.71 %	-3.75 %	-0.43 %	5.10 %	4.39 %	6.18 %	-2.73 %	-1.59 %	-1.04 %	7.54 %
D_3	-7.75 %	1.80 %	1.55 %	4.08 %	1.21 %	8.45 %	-7.50 %	-7.56 %	-8.33 %	-5.84 %
D_4	9.15 %	-9.36 %	-2.67 %	9.21 %	8.86 %	9.74 %	8.50 %	8.02 %	-5.21 %	5.60 %
D_5	-4.99 %	-2.03 %	6.29 %	5.71 %	5.53 %	5.98 %	-5.45 %	3.63 %	-7.29 %	-4.81 %

^a D_1 is calculated as (CG – Simulated) / Simulated, D_2 is calculated as (RGR – Simulated) / Simulated, D_3 is calculated as (Spline – Simulated) / Simulated, D_4 is calculated as (ETT – Simulated) / Simulated and D_5 is calculated as (EDMD – Simulated) / Simulated.

Table 4

The evaluation of the roughness components.

Unit (mm)	S_q	S_{sk}	S_{ku}	S_z	S_p	S_v	S_a	S_{dq}	S_{dr}	S_k
Simulated	0.0479	0.0618	3.0315	0.3286	0.1631	0.1655	0.0404	0.3949	0.0111	0.0585 ^a
CG	0.0437	0.0593	3.0053	0.3004	0.1507	0.1497	0.0369	0.3622	0.0101	0.0545
RGR	0.0442	0.0668	3.0755	0.2971	0.1469	0.1502	0.0365	0.3673	0.0103	0.0529
Spline	0.0493	0.0672	3.0686	0.3042	0.1524	0.1518	0.0394	0.3805	0.0106	0.0586
ETT	0.0457	0.0628	3.0663	0.3011	0.1496	0.1515	0.0367	0.3645	0.0102	0.0527
EDMD	0.0494	0.0672	3.002	0.3176	0.1488	0.1688	0.0393	0.3797	0.0118	0.0529
D_1	-8.77 %	-4.05 %	-0.86 %	-8.58 %	-7.60 %	-9.55 %	-8.66 %	-8.28 %	-9.01 %	-6.84 %
D_2	-7.72 %	8.09 %	1.45 %	-9.59 %	-9.93 %	-9.24 %	-9.65 %	-6.99 %	-7.21 %	-9.57 %
D_3	2.92 %	8.74 %	1.22 %	-7.43 %	-6.56 %	-8.28 %	-2.48 %	-3.65 %	-4.50 %	0.17 %
D_4	-4.59 %	1.62 %	1.15 %	-8.37 %	-8.28 %	-8.46 %	-9.16 %	-7.70 %	-8.11 %	-9.91 %
D_5	3.13 %	8.74 %	-0.97 %	-3.35 %	-8.77 %	1.99 %	-2.72 %	-3.85 %	6.31 %	-9.57 %

^a D_1 is calculated as (CG – Simulated) / Simulated, D_2 is calculated as (RGR – Simulated) / Simulated, D_3 is calculated as (Spline – Simulated) / Simulated, D_4 is calculated as (ETT – Simulated) / Simulated and D_5 is calculated as (EDMD – Simulated) / Simulated.

Step 4: Quantitative evaluation. Select evaluation area randomly and quantitatively analyze the filtering effectiveness by calculating the parameters of filtered surface components.

3.2. Data transforming

At present, the generally used measurement techniques are contact and noncontact measurement methods. In Fig. 2, a noncontact laser holographic interferometry measuring instrument called Coherix ShaPix is used to measure the engineering surface, which represents the three-dimensional surface by millions of data points. The instrument has a sampling accuracy of 1µm in the z direction and 150µm in the x and y direction. Hence the measured surface V_m is represented by millions of points. However, the measured points of V_m are redundant and discontinuous, which will affect the authenticity of surface data. To deal with the existing problem, the data preprocessing is required.

Firstly, the duplicate and outlier points are removed. For the purpose of surface inverse modeling in CAD software, the points need to be rearranged. During the measurement, the instrument is fixed in x direction and measures the height value of engineering surface along y

direction. Then, the positions in x direction are various and measuring the height value in the same way to obtain a series of the discrete data points $P = \{p_i = (x_i, y_i, z_i) | i = 1, 2, \dots, N\}$, which represents the measured engineering surface. Based on the measuring method, the data points can be rearranged by the order of two dimensional coordinates as follow cases with $i = 1, 2, \dots, N - 1$ and variable m is referred to the number of curves which initial value is one.

- Case1: if $|x_i - x_{i+1}| \leq 0.15$ and $|y_i - y_{i+1}| \leq 0.15$, then $p_i, p_{i+1} \in C_m$;
- Case2: if $|x_i - x_{i+1}| \leq 0.15$ and $|y_i - y_{i+1}| > 0.15$, then $p_i \in C_m, p_{i+1} \in C_{m+1}, m = m + 1$;
- Case3: if $|x_i - x_{i+1}| > 0.15$, then $p_i \in C_m, p_{i+1} \in C_{m+1}, m = m + 1$;

Finally, the rearranged file is exported for surface inverse modeling. According to the method of point's rearrangement, an example of the point's rearrangement is given in Fig. 3.

Example 1. One set M which contains 20 points. According to the x-axis and y-axis coordinates of points, set M is sorted as set $M_1 = \{p_i | p_i = (x_i, y_i, z_i), i = 1, 2, \dots, 20\}$.

$$M = \{(0.05, 0, 0.1), (0.21, 0, 0.3), (0.35, 0, 0.1), (0.8, 0, 0.1), (0.05, 0.1, 0.2), (0.21, 0.1, 0.2), (0.35, 0.1, 0.2), (0.8, 0.1, 0.2), (0.05, 0.2, 0.2), (0.26, 0.25, 0.1), (0.35, 0.25, 0.3), (0.8, 0.2, 0.2), (0.05, 0.31, 0.1), (0.05, 0.4, 0.2), (0.26, 0.45, 0.2), (0.26, 0.55, 0.3), (0.55, 0.25, 0.2), (0.65, 0.4, 0.1), (0.85, 0.31, 0.1), (0.85, 0.4, 0.2)\} \tag{6}$$

$$M_1 = \{(0.05, 0, 0.1), (0.05, 0.1, 0.2), (0.05, 0.2, 0.2), (0.05, 0.31, 0.1), (0.05, 0.4, 0.2), (0.21, 0, 0.3), (0.21, 0.1, 0.2), (0.26, 0.25, 0.1), (0.26, 0.45, 0.2), (0.26, 0.55, 0.3), (0.35, 0, 0.1), (0.35, 0.1, 0.2), (0.35, 0.25, 0.3), (0.55, 0.25, 0.2), (0.65, 0.4, 0.1), (0.8, 0, 0.1), (0.8, 0.1, 0.2), (0.8, 0.2, 0.2), (0.85, 0.31, 0.1), (0.85, 0.4, 0.2)\} \tag{7}$$

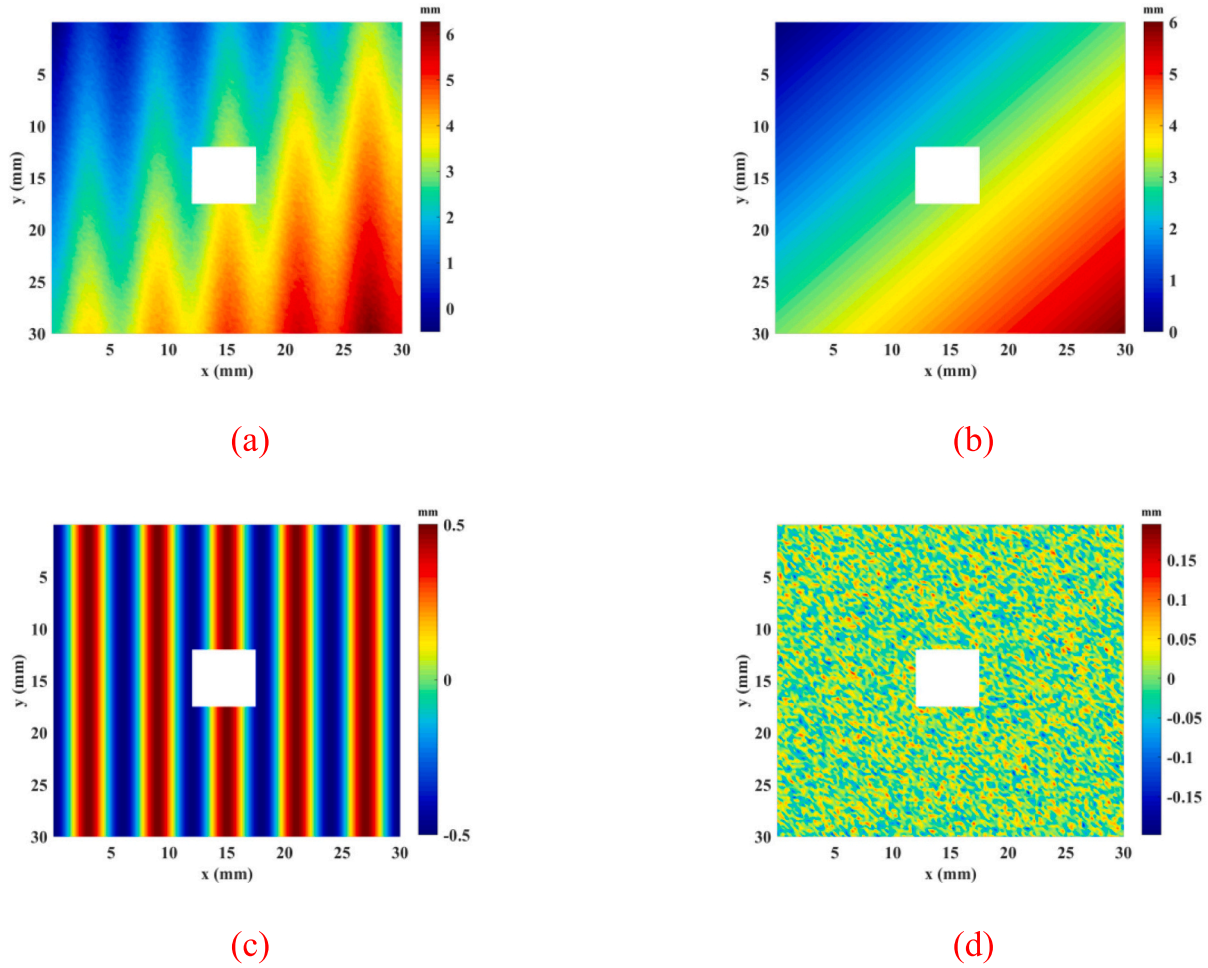


Fig. 12. All components of the discontinuous simulated surface (a) the original simulated surface (b) form component (c) waviness component (d) roughness component.

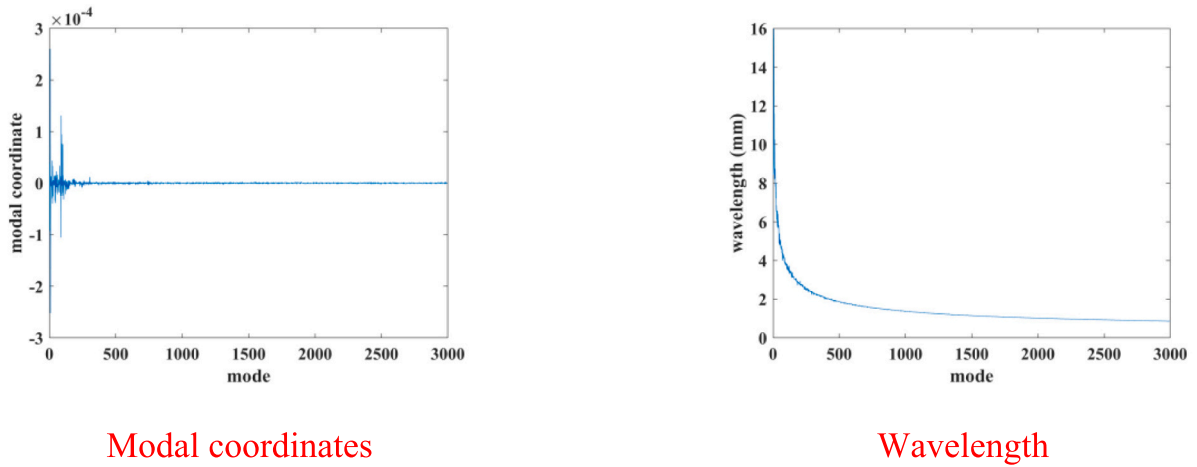


Fig. 13. The modal coordinates and the wavelengths.

Based on the principle of rearranging points, the points can be grouped to six curves which are shown in Fig. 3(b) and (c).

3.3. Surface inverse modeling

The step of surface inverse modeling is completed in CAD software

using triangular mesh. Import the rearranged file to CAD software, and multiple curves will be generated and displayed. The surface model V_s can be inversely reconstructed by curve-surface fitting using the boundary blending function. The inverse modeling process does not change the positions and heights of the measured points, thereby preserving surface texture and roughness.

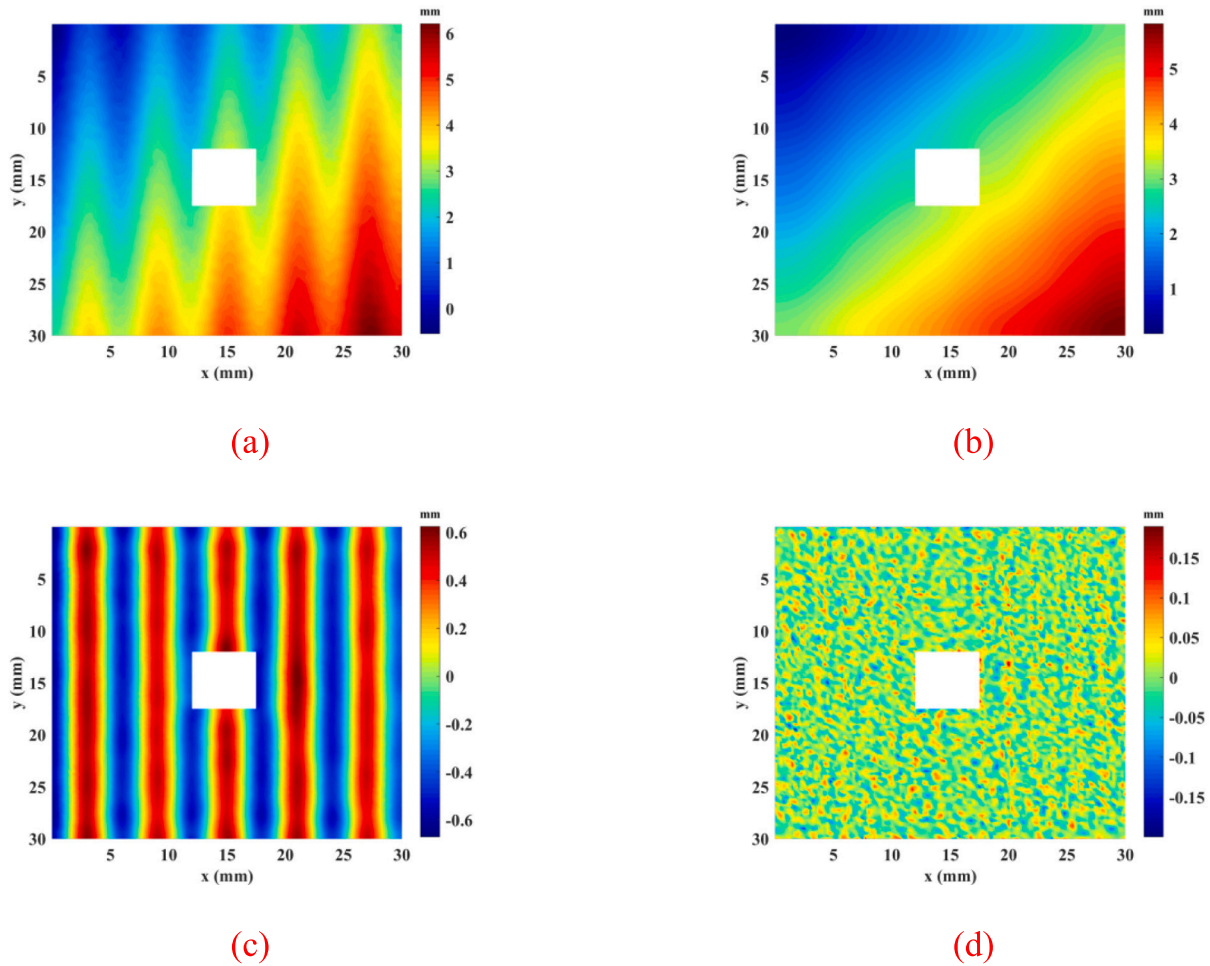


Fig. 14. The filtering results of EDMD method (a) the reconstructed surface (b) form component (c) waviness component (d) roughness component.

Example 2. A surface inverse modeling example is shown in Fig. 4. According to the rearrange principle, 961 points are rearranged and 31 curves are generated. As shown in Fig. 4(b), the surface is generated by curves.

3.4. Extended discrete modal decomposition

As description above (see Section 2), each extracted mode by DMD has not been defined the physical dimension. To establish the relationship between extracted modes and surface components, the extended discrete modal decomposition (EDMD) is proposed. The EDMD method can be separated into four modules: modal decomposition, DMD calculation, two dimensional Hilbert transform, and modal recombination. Fig. 5 presents the entire EDMD process, which shows the comparison with the DMD method. The specific modules are as follows.

Module 1: modal decomposition

Import the surface model V_s for modal decomposition. Firstly, set the properties and the degree of freedom of engineering surface. Then, the lanczos eigensolver are applied to modal decomposition and the surface model V_s are decomposed into a set of descriptors obtaining from the mechanical dynamics, which form the modal basis Q . After completing modal decomposition, the mass matrix M and the stiffness matrix K are exported for DMD calculation.

Example 3. A 30 mm × 30 mm square surface is generated as an example. Setting the properties of surface and leaving one degree of

freedom in z direction. After completing modal decomposition, some modal bases are shown in Fig. 6.

Module 2: DMD calculation

DMD calculation is derived from a structural dynamic problem. As explained in Section 2, modal basis Q can be calculated from the mass matrix M and the stiffness matrix K . The modal contributions (or modal coordinates) λ refer to original shape mapping to modal space, which are available through the modal basis Q and the surface V_m (see Eq. (4)). Since the modes are ordered according to the vibration frequencies after modal decomposition, different scale surface components can be obtained from the combination of modes with different modal alignment intervals respectively.

Module 3: two dimensional Hilbert transform

The multi-scale surface components are generally classified by wavelengths from small scale to large scale. Refer to ISO 4287 [36], λ_s , λ_c and λ_f respectively denote the cutoff wavelength of roughness, waviness and form component. However, the wavelength interval among primary form, waviness and roughness in DMD has not been explicitly mapped to the decomposed modes. To build the relationship, two dimensional Hilbert transform is applied to identify the wavelength of each mode in physical dimensions. By means of the wavelengths obtained from the two dimensional Hilbert transform, the modes can be combined into each surface component with reference to the standard. Therefore, it is important to calculate the wavelength of the extracted modes.

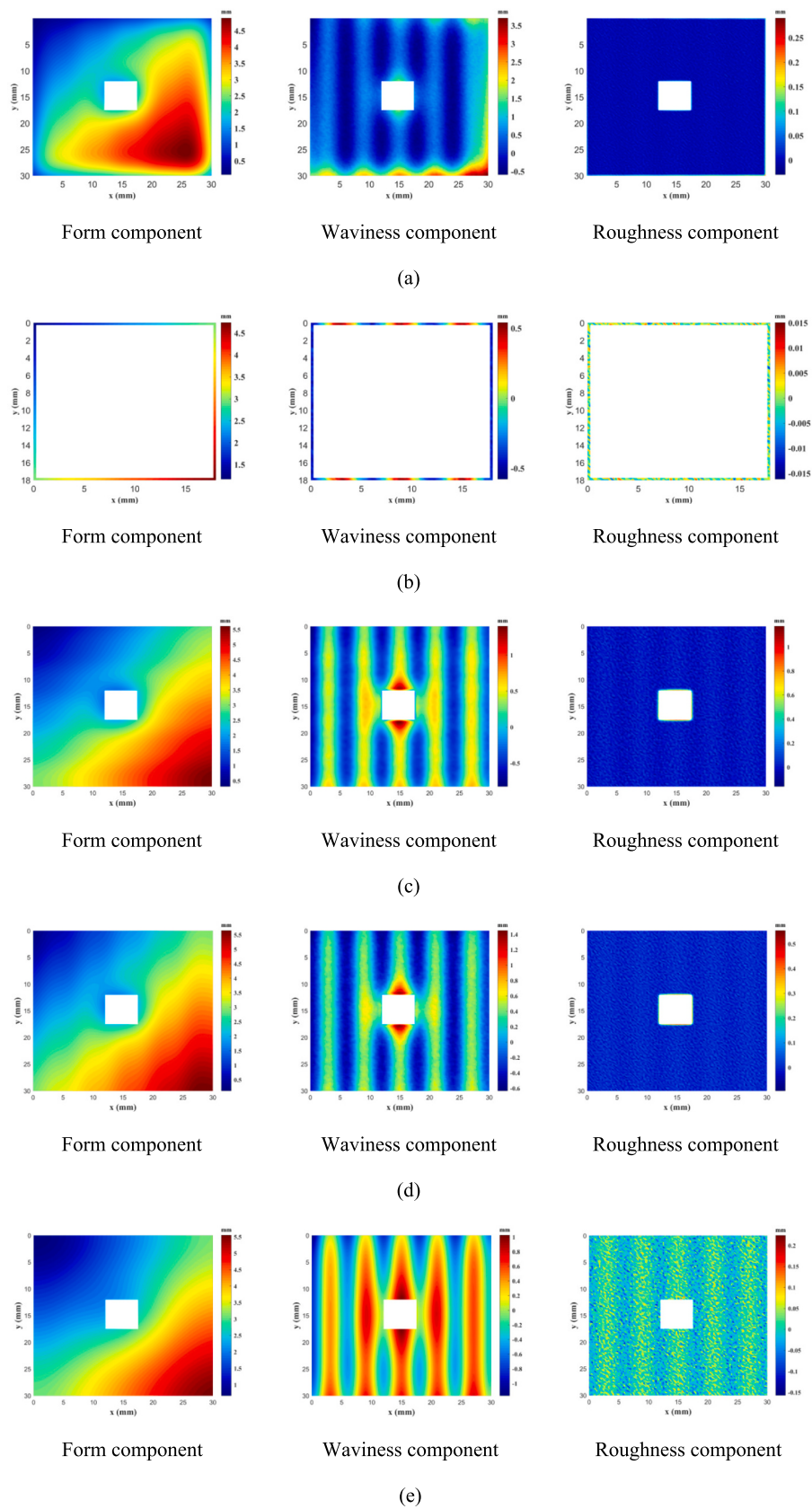


Fig. 15. The filtering results (a) Gaussian filter (b) Cutoff Gaussian filter (c) robust Gaussian regression filter (d) spline filter (e) extended tetrolet transform.

Table 5
The evaluation of the waviness components.

Unit (mm)	S_q	S_{sk}	S_{ku}	S_z	S_p	S_v	S_a	S_{dq}	S_{dr}	S_k
Simulated	0.342	0.1992	1.6131	1	0.5536	0.4464	0.3052	0.3729	0.0104	0.5453 ^a
Gaussian	0.3851	0.5822	2.9644	1.7679	1.1908	0.577	0.3148	0.5008	0.0143	0.496
RGR	0.3996	0.496	2.7674	1.8547	1.199	0.6557	0.3302	0.5172	0.0148	0.5348
Spline	0.3518	0.1671	2.0264	1.4899	0.7748	0.7151	0.302	0.487	0.0139	0.5127
ETT	0.3818	0.1625	2.0628	1.5689	0.8581	0.7108	0.326	0.387	0.0108	0.5465
EDMD	0.3345	0.1797	1.7137	1.0515	0.5745	0.477	0.2932	0.3652	0.0096	0.512
D_1	12.60 %	192.27 %	83.77 %	76.79 %	115.10 %	29.26 %	3.15 %	34.30 %	37.50 %	-9.04 %
D_2	16.84 %	149.00 %	71.56 %	85.47 %	116.58 %	46.89 %	8.19 %	38.70 %	42.31 %	-1.93 %
D_3	2.87 %	-16.11 %	25.62 %	48.99 %	39.96 %	60.19 %	-1.05 %	30.60 %	33.65 %	-5.98 %
D_4	11.64 %	-18.42 %	27.88 %	56.89 %	55.00 %	59.23 %	6.82 %	3.78 %	3.85 %	0.22 %
D_5	-2.19 %	-9.79 %	6.24 %	5.15 %	3.78 %	6.85 %	-3.93 %	-2.06 %	-7.69 %	-6.11 %

^a D_1 is calculated as (Gaussian – Simulated) / Simulated, D_2 is calculated as (RGR – Simulated) / Simulated, D_3 is calculated as (Spline – Simulated) / Simulated, D_4 is calculated as (ETT – Simulated) / Simulated and D_5 is calculated as (EDMD – Simulated) / Simulated.

Table 6
The evaluation of the roughness components.

Unit (mm)	S_q	S_{sk}	S_{ku}	S_z	S_p	S_v	S_a	S_{dq}	S_{dr}	S_k
Simulated	0.0499	0.0618	2.8453	0.3189	0.1651	0.1538	0.0402	0.3949	0.0111	0.0626 ^a
Gaussian	0.168	0.5145	2.2867	2.2136	0.9471	1.2665	0.0677	1.0617	0.0313	0.0547
RGR	0.1179	0.5531	3.8469	1.0862	0.9315	0.1547	0.0537	0.5199	0.0149	0.0391
Spline	0.1402	0.50141	3.8396	1.2402	1.0578	0.1824	0.0661	0.5083	0.0145	0.0412
ETT	0.0453	0.0486	2.9286	0.2828	0.1566	0.1263	0.0363	0.3687	0.0103	0.0538
EDMD	0.0484	0.0679	2.9197	0.304	0.1519	0.1521	0.0384	0.3895	0.0103	0.0614
D_1	236.67 %	732.52 %	-19.63 %	594.14 %	473.65 %	723.47 %	68.41 %	168.85 %	181.98 %	-12.62 %
D_2	136.27 %	794.98 %	35.20 %	240.61 %	464.20 %	0.59 %	33.58 %	31.65 %	34.23 %	-37.54 %
D_3	180.96 %	711.34 %	34.95 %	288.90 %	540.70 %	18.60 %	64.43 %	28.72 %	30.63 %	-34.19 %
D_4	-9.22 %	-21.36 %	2.93 %	-11.32 %	-5.15 %	-17.88 %	-9.70 %	-6.63 %	-7.21 %	-14.06 %
D_5	-3.01 %	9.87 %	2.61 %	-4.67 %	-8.00 %	-1.11 %	-4.48 %	-1.37 %	-7.21 %	-1.92 %

^a D_1 is calculated as (Gaussian – Simulated) / Simulated, D_2 is calculated as (RGR – Simulated) / Simulated, D_3 is calculated as (Spline – Simulated) / Simulated, D_4 is calculated as (ETT – Simulated) / Simulated and D_5 is calculated as (EDMD – Simulated) / Simulated.

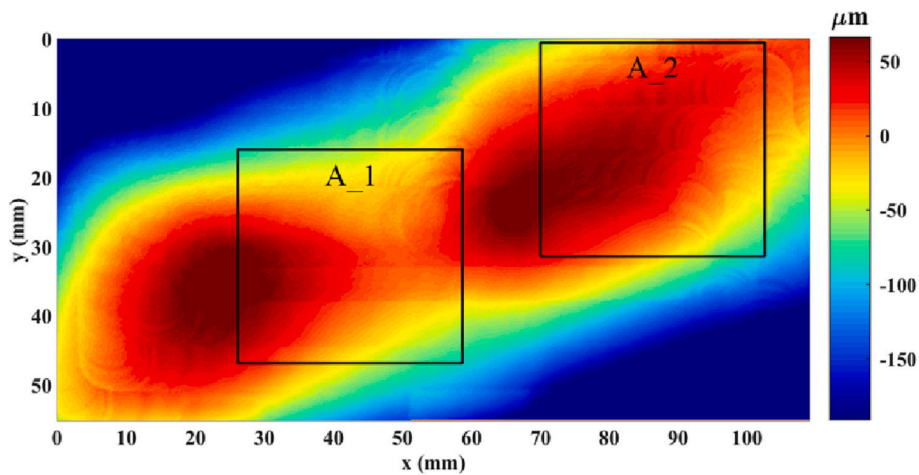


Fig. 16. The two dimensional diagram of the phone back surface.

Two dimensional Hilbert transform is based on monogenic signal theory [37]. Each modal displacement is assumed to a small and harmonic solution of equation as

$$P_i(x, y) = f_i(x, y) \cos(\varphi_i(x, y)) \tag{8}$$

where $f_i(x, y) = \lambda_i Q_i(x, y)$ is the instantaneous amplitude of the discrete mode f_i , $\varphi_i(x, y)$ and $\varphi_i'(x, y)$ are the phase and frequency respectively.

Subsequently, according to the Two dimensional Hilbert transform and vector field theory, the monogenic signal $P_{iM}(x, y)$ can be obtained:

$$P_{iM}(x, y) = (P_i(x, y), -P_{iR}(x, y))^T \tag{9}$$

$$P_{iR}(x, y) = P_i(x, y) * h(x, y) \tag{10}$$

$$h(x, y) = \left(-x / \sqrt{2\pi(x^2 + y^2)^{3/2}}, -y / \sqrt{2\pi(x^2 + y^2)^{3/2}} \right) \tag{11}$$

where $P_{iR}(x, y)$ is the two dimensional Hilbert transform of $P_i(x, y)$, * Represents convolutional operation and $h(x, y)$ is the two dimensional Hilbert transform convolutional kernel. Converting the monogenic signal $P_{iM}(x, y)$ into polar coordinates, the amplitude $A_i(x, y)$, the phase $l_{ip}(x, y)$ and the frequency $l_{if}(x, y)$ can be calculated as:

$$A_i(x, y) = \|P_{iM}(x, y)\| = \sqrt{P_i^2(x, y) + \|P_{iR}(x, y)\|^2} \tag{12}$$

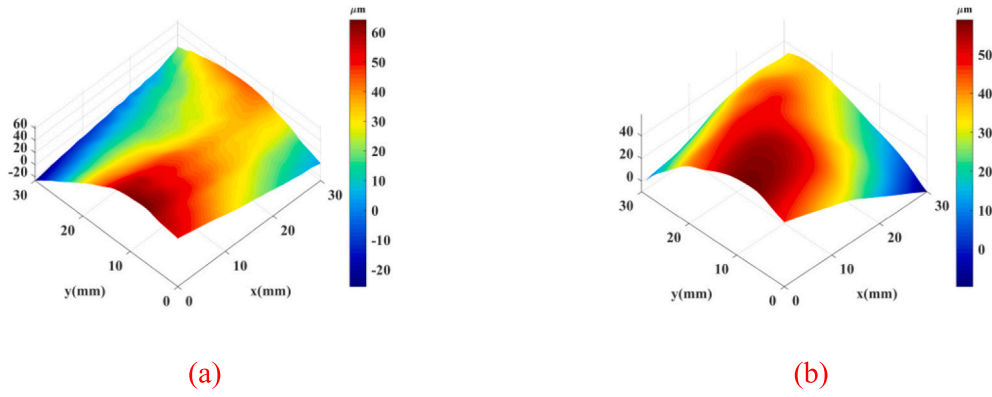
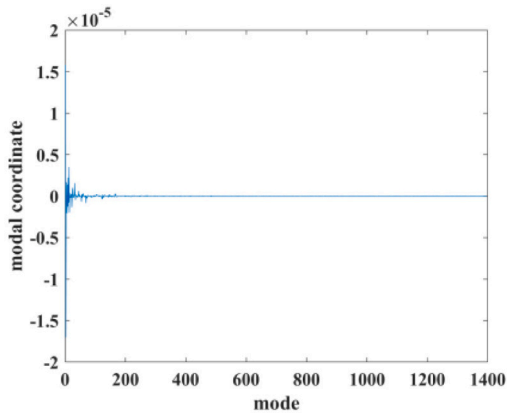
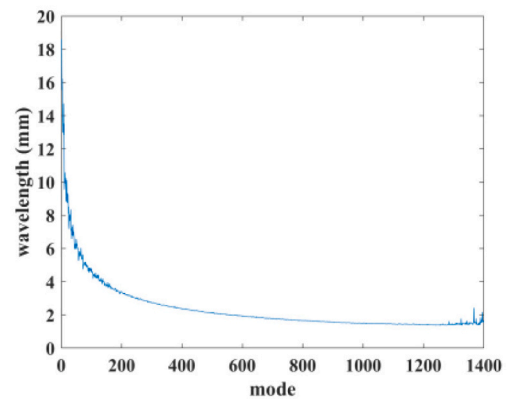


Fig. 17. The original surfaces (a) surface A_1 (b) surface A_2.

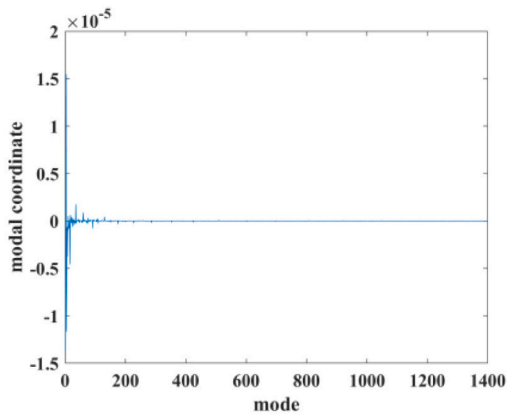


Modal coordinates

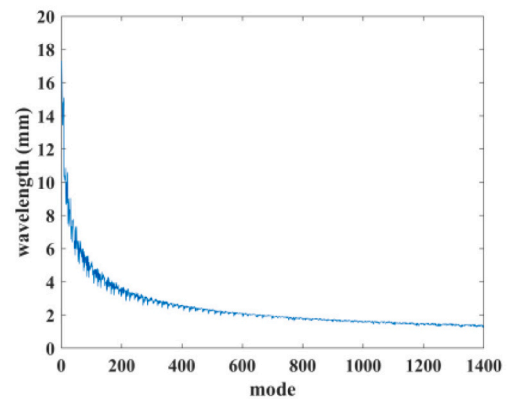


Wavelengths

(a)



Modal coordinates



Wavelengths

(b)

Fig. 18. The modal coordinates and the wavelengths (a) surface A_1 (b) surface A_2.

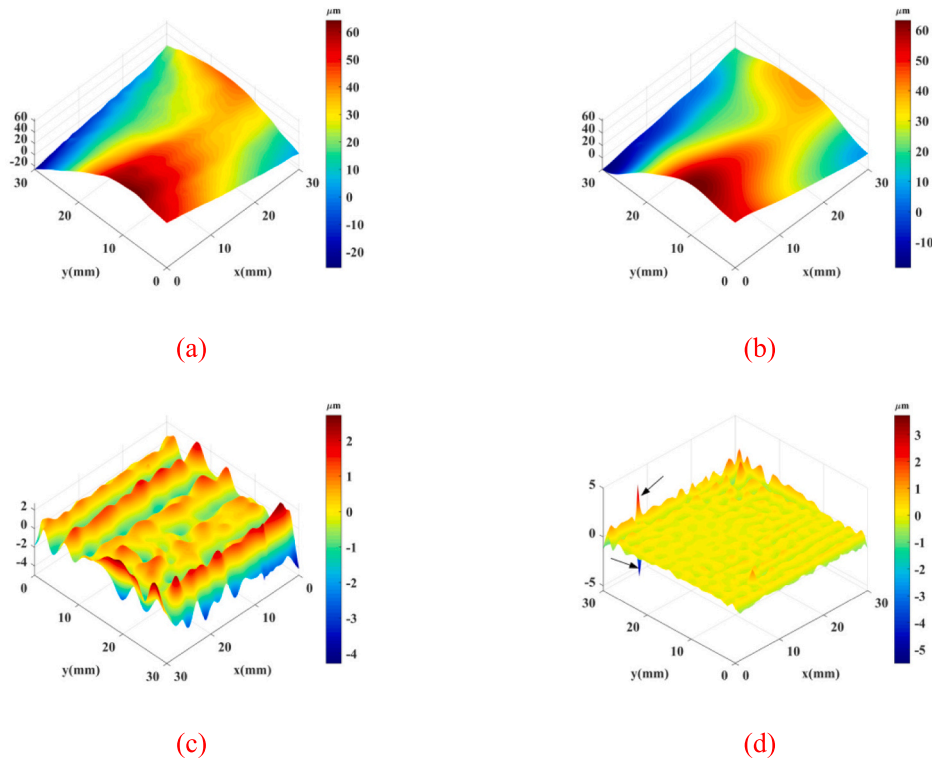


Fig. 19. The filtering result of surface A_1 (a) the surface reconstructed by first 1400 modes (b) form component (c) waviness component (d) roughness component.

$$l_{ip}(x, y) = \arctan2(P_i(x, y), P_{iR}(x, y)) \tag{13}$$

$$l_{if}(x, y) = \sqrt{\left(\frac{\partial l_{ip}(x, y)}{\partial x}\right)^2 + \left(\frac{\partial l_{ip}(x, y)}{\partial y}\right)^2} \tag{14}$$

Afterwards, the wavelength $\lambda = \{\lambda_{1k}, \lambda_{2k}, \lambda_{3k}, \dots, \lambda_{Nk}\}$ of the discrete modes can be calculated through the relationship between frequency and wavelength in physics.

$$\lambda_{ik} = x_1 y_1 \left(\sum_{x=1}^{x_1} \sum_{y=1}^{y_1} l_{if}(x, y) \right)^{-1} \quad (i = 1, 2, \dots, N) \tag{15}$$

where x_1 and y_1 represent the points number on the direction of x and y .

Module 4: modal combination

After calculating all modes' wavelengths information λ_{ik} ($i = 0, 1, \dots, N$), discrete modes can be combined as the principle show in Table 1.

The process of the specific discrete mode combine to the different scale component is carried out by discrete modal decomposition theory. The combined method is listed as below:

$$V_f = \sum_{i=1}^j f_i(x, y) = \sum_{i=1}^j \lambda_i Q_i(x, y) \tag{16}$$

$$V_w = \sum_{i=j+1}^k f_i(x, y) = \sum_{i=j+1}^k \lambda_i Q_i(x, y) \tag{17}$$

$$V_r = \sum_{i=k+1}^m f_i(x, y) = \sum_{i=k+1}^m \lambda_i Q_i(x, y) \tag{18}$$

where λ_i is the modal coordinates (or modal contributions), Q_i is vector of the modal basis, V_f represents form component, V_w represents waviness component and V_r represents roughness component.

3.5. Quantitative evaluation

To quantitatively evaluate the EDMD method performance, areal surface parameters is adopted to analyze the filtered surface components. According to the latest standard ISO 25178-2 [38], the height parameters ($S_q, S_p, S_v, S_z, S_a, S_{sk}, S_{ku}$), the hybrid parameters (S_{dq}, S_{dr}) and functional parameters S_k are selected. These parameters are listed in Table 2.

4. Numerical simulation

In order to validate the effectiveness of EDMD method, a continuous simulated surface and a discontinuous simulated surface are constructed through the equation shown as follows.

$$S(x, y) = 0.1x + 0.1y - 0.5\cos(2\pi x/6) + 0.5 \times \text{normrnd}(0, 0.1) \tag{19}$$

where the linear term ($0.1x + 0.1y$) represents form component, the cosine term ($0.5 \cos(2\pi x/6)$) represents waviness component, and the rest term ($0.5 \times \text{normrnd}(0, 0.1)$) generate a Gaussian distribution matrix which represents roughness component. The sampling spacing of the simulated surface is 0.25 mm, and 121×121 sampling points are generated to makeup the $30 \text{ mm} \times 30 \text{ mm}$ sampling area. A square with 5 mm sides is removed from the center of continuous surface to generate the discontinuous surface. The results of the inverse modeling are shown in Fig. 7. Gaussian filter, robust Gaussian regression filter and spline filter are generally acknowledged standard filter methods. The extended tetrolet transform [28] is the recently proposed filtering method for surfaces with holes. For comparisons, the simulated surfaces are filtered by Gaussian filter, Cutoff Gaussian filter (CG), robust Gaussian regression filter (RGR), spline filter, extended tetrolet transform (ETT) and the EDMD method, respectively.

4.1. Continuous simulated surface

During the decompose process using EDMD method, the fixed

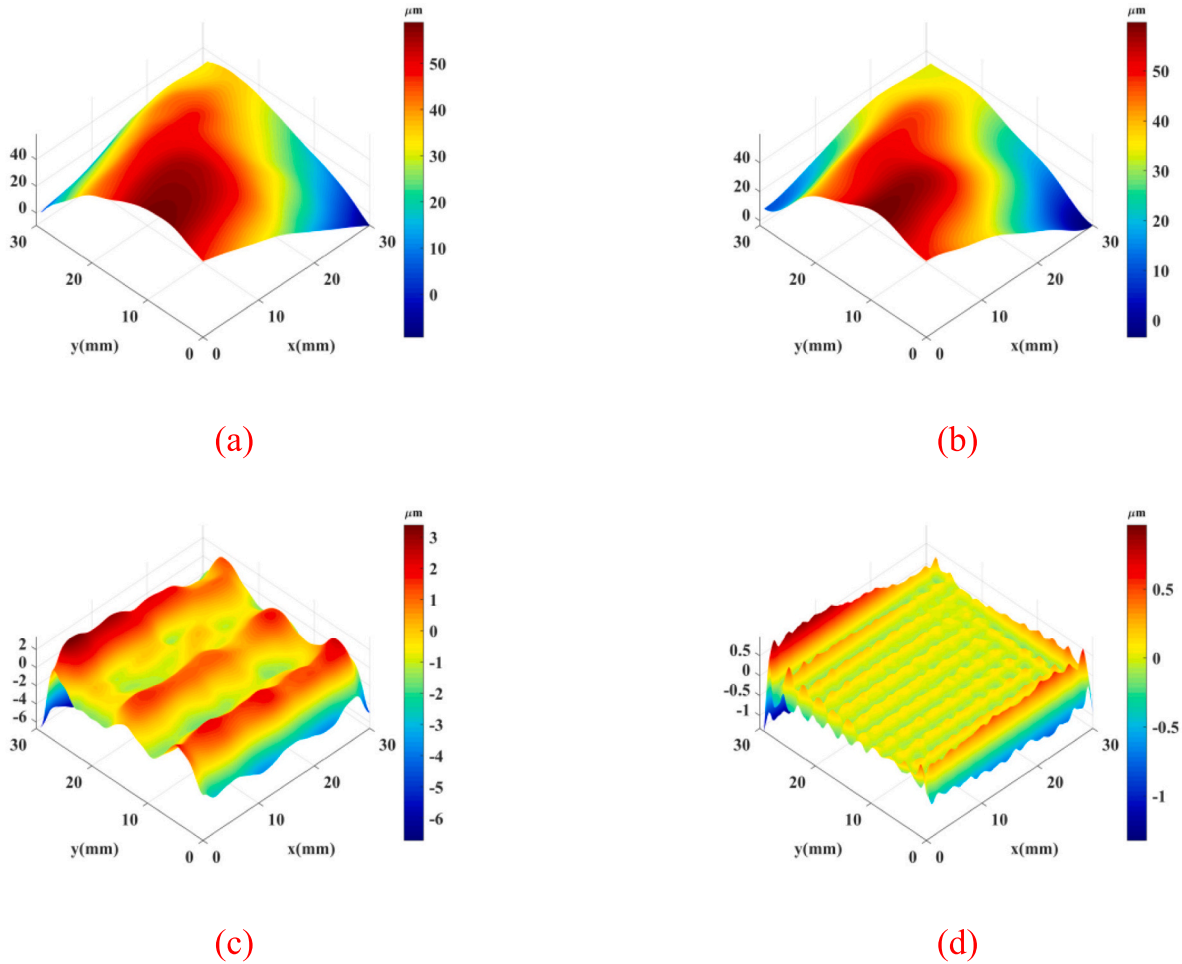


Fig. 20. The filtering result of surface A_2 (a) the surface Reconstructed by first 1400 modes (b) form component (c) waviness component (d) roughness component.

Table 7
Quantitative evaluations for waviness and roughness components.

Unit (mm)	S_q	S_{sk}	S_{ku}	S_z	S_p	S_v	S_a	S_{dq}	S_{dr}	S_k
A_1_Waviness	0.873	-0.0354	3.558	6.911	2.706	4.205	0.698	0.357	0.015	1.0581
A_1_Roughness	0.307	-0.012	9.415	9.784	3.770	6.014	0.213	0.369	0.021	0.3105
A_2_Waviness	1.401	-1.029	5.781	9.362	3.015	6.347	1.043	0.372	0.018	1.309
A_2_Roughness	0.186	-0.681	12.073	2.015	0.984	1.061	0.110	0.384	0.016	0.1158

Table 8
The measurement comparison results of roughness.

Unit (mm)	R_q	R_{sk}	R_{ku}	R_z	R_p	R_v	R_a
A_1	0.293	-0.010	9.32	9.511	3.601	5.91	0.199 ^a
A_2	0.193	-0.686	12.252	1.965	0.991	0.974	0.105
D_A_1	0.014	-0.002	0.095	0.273	0.169	0.104	0.014
D_A_2	-0.007	0.005	-0.179	0.050	-0.007	0.087	0.005

^a D_A_1 is calculated as (A_1_Roughness - A_1) and D_A_2 is calculated as (A_2_Roughness - A_2).

boundary is applied to the surface which leaves one degree of freedom in z direction. Fig. 8 shows all of the continuous surface components.

For purpose of filtering the deviations caused by the modes of low amplitude and high frequency, the surface is selected the first 3000 modes for the subsequent analysis. The modal coordinates after modal decomposition is shown in Fig. 9(a). It can be seen that the modal coordinates have a large variation in the first few orders, and with less

fluctuation thereafter. The wavelengths of the first 3000 modes obtain by two dimensional Hilbert transform is shown in Fig. 9(b). It is obvious that the slope of the curve of the wavelength decreases as the mode increases, especially in the first few orders of modes where it decreases fastest. Refer to ISO 25178-3 [39], the cutoff wavelengths $\lambda_s = 0.0025mm$, $\lambda_c = 2.5mm$ and $\lambda_f = 8mm$ are adopted. Based on the solved wavelengths and the modal combination principle, form, waviness and roughness components are combined by modes $\{f_i(x,y)|i = 1, 2, \dots, 32\}$, $\{f_i(x,y)|i = 33, 34, \dots, 402\}$ and $\{f_i(x,y)|i = 403, 404, \dots, 3000\}$ respectively. Fig. 10 shows the results of recombination by modes $\{f_i(x,y)|i = 1, 2, \dots, 3000\}$ and the filtered surface components. It is clear that the EDMD method can separate the simulated surface to different scale components without end effect.

For comparison, Gaussian filter, Cutoff Gaussian filter (CG), robust Gaussian regression filter (RGR), spline filter and extended tetrolet transform (ETT) are also applied to the simulated surface. As shown in Fig. 11(a), the border distortion of the filtered surface components by Gaussian filter is obvious. Cutoff Gaussian filter is generated by selecting a specific area of Gaussian filter. As shown in Fig. 11(b), Cutoff Gaussian

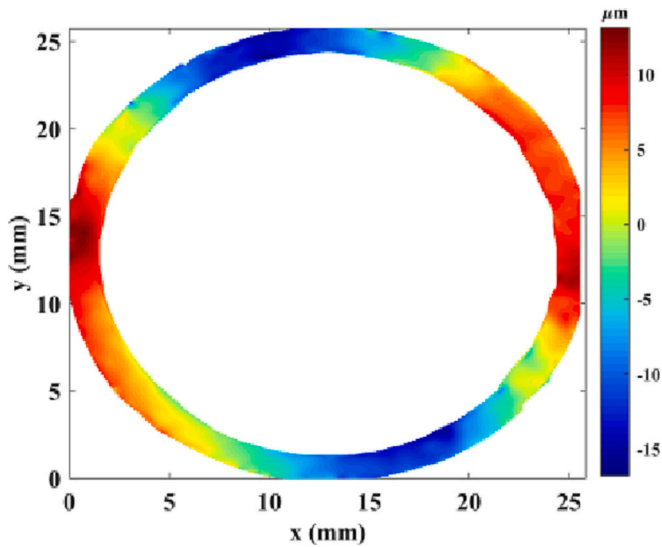


Fig. 21. The two dimensional diagram of the pump spool bore surface.

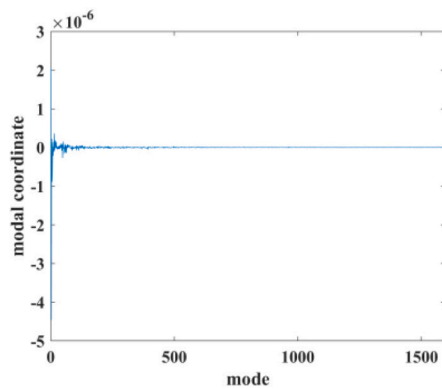
filter subtracts the length of 6 mm at the boundary to reduce the border distortion. The filtering result of robust Gaussian regression filter, spline filter and extended tetrolet transform are shown in Fig. 11 (c), (d) and (e), respectively. The visualization results indicate that robust Gaussian regression filter, spline filter and extended tetrolet transform can also well separate the surface components and reduce the end effect.

Then, the quantitative evaluation (see Section 3.5) is applied to simulated surface components and filtered surface components. The evaluation rules [38] require that the dimension of evaluating area is not less than the cutoff wavelength. Hence, quantitative evaluation is applied within a same 8 mm × 8 mm area. The evaluation results of waviness and roughness component are shown in Tables 3 and 4. The differences of the five methods compare with the simulated surface

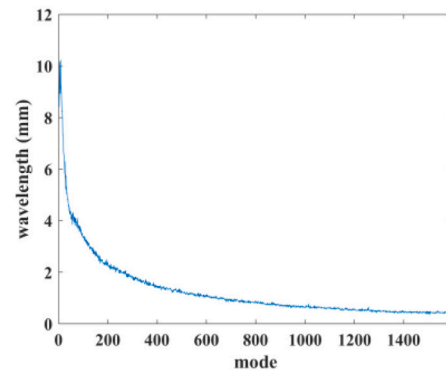
Table 10
The measurement comparison results of roughness.

Unit (mm)	R_q	R_{sk}	R_{ku}	R_z	R_p	R_v	R_a
Case 2	0.124	-0.166	4.739	3.153	1.219	1.934	0.118 ^a
D	-0.012	0.014	0.242	0.083	-0.088	0.171	-0.034

^a D is calculated as (Case 2 – Roughness).



Modal coordinates



Wavelengths

Fig. 22. The modal coordinates and the wavelengths.

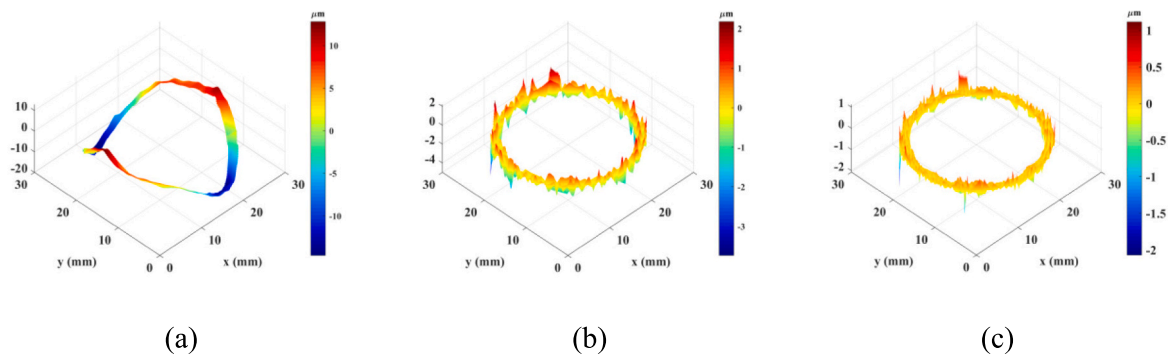


Fig. 23. The filtering results of the surface (a) form component (b) waviness component (c) roughness component.

Table 9
Quantitative evaluations for waviness and roughness components.

Unit (mm)	S_q	S_{sk}	S_{ku}	S_z	S_p	S_v	S_a	S_{dq}	S_{dr}	S_k
Waviness	0.452	-0.418	5.172	5.674	2.160	3.514	0.336	0.272	0.021	0.418
Roughness	0.112	-0.152	4.981	3.236	1.131	2.105	0.084	0.298	0.026	0.101

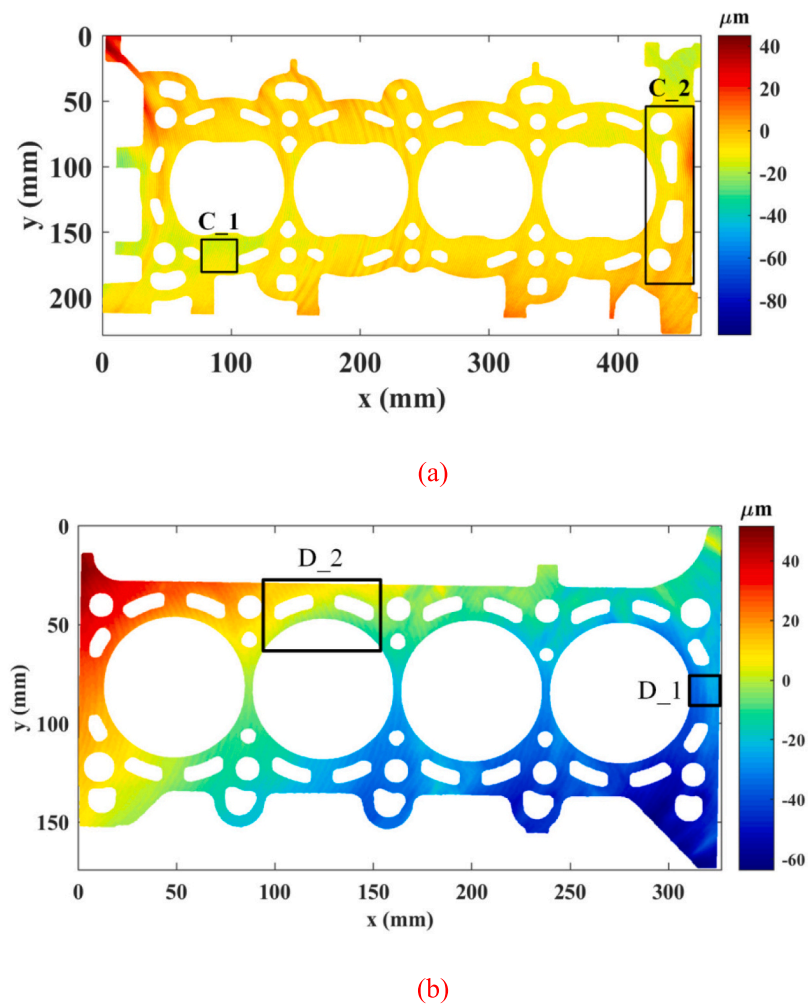


Fig. 24. The two dimensional diagram of engineering surfaces (a) engine cylinder head (b) engine cylinder block.

components are approximate and all within 10%. It can be considered as normal deviations which demonstrate the separated components are no distortions and the EDM method is feasible for surface filtering without end effect.

4.2. Discontinuous simulated surface

A square with 10 mm sides is removed from the center of continuous surface to generate the discontinuous simulated surface. Fig. 12 shows all of the discontinuous surface components. As same as continuous surface, the fixed boundary is used and selected the surface the first 3000 modes to analysis.

The modal coordinates and the wavelengths of the modes are shown in Fig. 13. The form, waviness and roughness components are combined by modes $\{f_i(x,y)|i = 1, 2, \dots, 38\}$, $\{f_i(x,y)|i = 39, 40, \dots, 352\}$ and $\{f_i(x,y)|i = 353, 354, \dots, 3000\}$ respectively. Fig. 14 presents the results of combination of modes $\{f_i(x,y)|i = 1, 2, \dots, 3000\}$ and the filtered surface components. The results demonstrate that the EDM method can effectively achieve the filtering of the discontinuous surface.

Analogously, the three filtering methods are compared in the discontinuous simulated surface, and the filtering result is shown in Fig. 15. It can be seen that Gaussian filter, Cutoff Gaussian filter, robust Gaussian regression filter and spline filter are not suitable for surface with holes due to the serious distortion at the boundary. After subtracting the length of 6 mm at the boundary, the Cutoff Gaussian filter is also failure to work. The end effect is reduced in the extended tetrolet

transform, but the little block effect occurs due to the constitution of tetrominoes, which cannot be overcome for the intrinsic property of tetrolet transform.

Furthermore, the same 8 mm × 8 mm area is selected randomly to quantitative analysis, and the results are shown in Tables 5 and 6. It is clear that large deviations appeared in Gaussian filter, robust Gaussian regression filter and Spline filter. The boundary of the hole appears slightly distorted using extended tetrolet transform. However, the EDM method still performs well which deviations are all within 10%. The results indicate Gaussian filter, cutoff Gaussian filter, robust Gaussian regression filter, spline filter, extended tetrolet transform exist the end effect when deal with the surface with a hole, and the EDM method can still overcome the end effect arises at the boundary of the hole.

Hence, it can be further derived that the EDM method has similar performance with the four filtering methods for continuous surface separation, and the EDM method is superior to the four methods for discontinuous surface filtering.

5. Case studies

5.1. Case study I

A phone back surface which represents a continuous surface is analyzed in the first case. The surface is made of aluminum alloy 7075 and Fig. 16 shows its two dimensional diagram. The geometrical

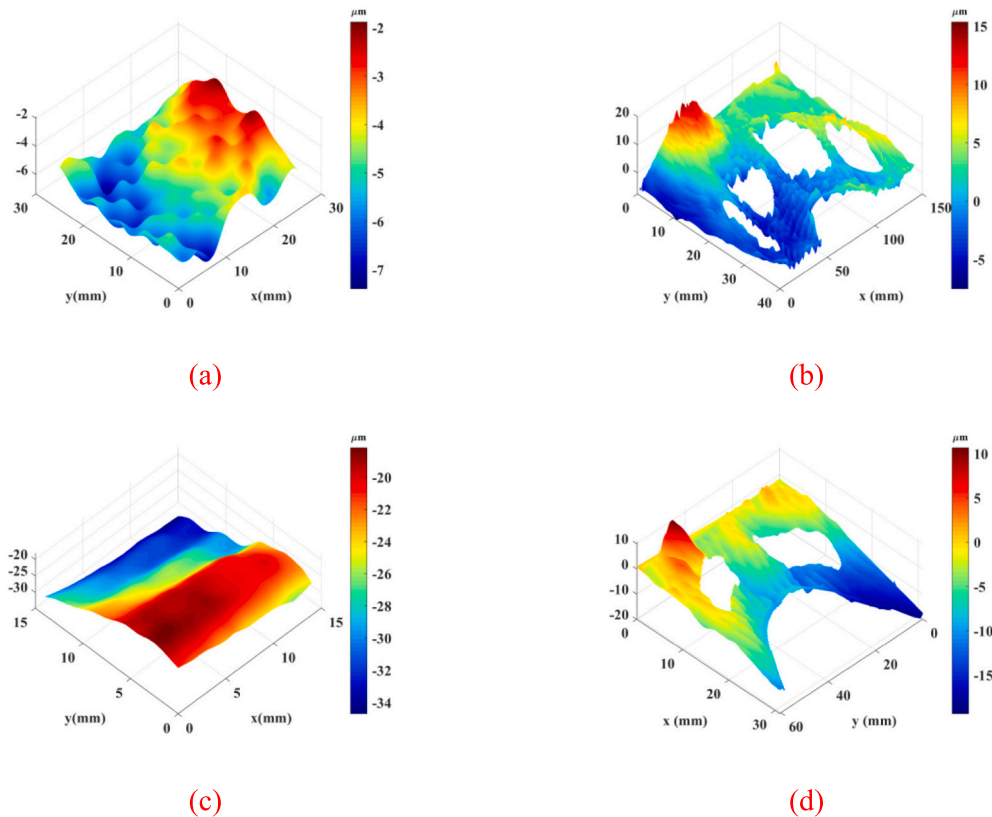


Fig. 25. The original surfaces (a) surface C_1 (b) surface C_2 (c) surface D_1 (d) surface D_2.

specification standard as $R_a = 3.2\mu\text{m}$, $R_z = 6.3\mu\text{m}$ and $W_t = 10\mu\text{m}$ are adopted. According to ISO 25178-3, the cutoff wavelengths are $\lambda_s = 0.008\text{mm}$, $\lambda_c = 2.5\text{mm}$ and $\lambda_f = 8\text{mm}$. Two random $30\text{ mm} \times 30\text{ mm}$ areal surfaces (namely A_1 and A_2 in Fig. 16) are selected for analysis using the EDMD method, and the original surfaces are shown in Fig. 17. The first 1400 modes of modal coordinates and the physical wavelengths of the two surfaces are shown in Fig. 18. Therefore, according to the wavelength of each mode, the modes can be combined to three surface components. For surface A_1, the form, waviness and roughness components are combined by modes $\{f_i(x,y)|i = 1, 2, \dots, 36\}$, $\{f_i(x,y)|i = 37, 38, \dots, 378\}$ and $\{f_i(x,y)|i = 379, 380, \dots, 1400\}$ respectively (see Fig. 19). For surface A_2, the form, waviness and roughness components are combined by modes $\{f_i(x,y)|i = 1, 2, \dots, 28\}$, $\{f_i(x,y)|i = 29, 30, \dots, 423\}$ and $\{f_i(x,y)|i = 424, 425, \dots, 1400\}$ respectively (see Fig. 20).

Moreover, the quantitative evaluation is applied to the two randomly selected surfaces in Table 7. In order to validate the availability of the proposed EDMD method, the measurement experiment using a Talysurf roughmeter is applied to the parts' surfaces and the results are shown in Table 8. The measured results are close to the actual results which illustrates the EDMD method is effectiveness. It is clear that the roughness parameter S_z of A_1 is greater than $6.3\mu\text{m}$ (Bold values in Tables 7 and 8), which beyond the geometrical specification standard, and it indicates the tool vibration and friction may occur during the manufacturing processes.

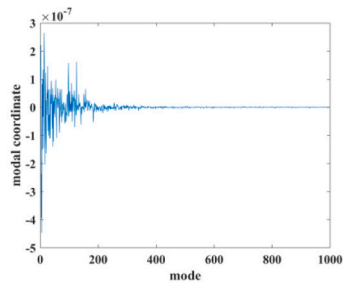
5.2. Case study II

A pump spool bore surface with a single hole made of Gray cast iron is analyzed in this case, and Fig. 21 shows its two dimensional diagram. The geometrical specification standard as $R_a = 1.6\mu\text{m}$, $R_z = 6.3\mu\text{m}$ and $W_t = 10\mu\text{m}$ are adopted and the cutoff wavelengths are $\lambda_s = 0.0025\text{mm}$, $\lambda_c = 0.8\text{mm}$ and $\lambda_f = 2.5\text{mm}$ respectively. As shown in Fig. 22, the modal

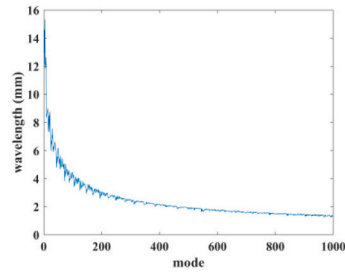
coordinates and the wavelengths of the first 1600 modes are calculated. The modal combination results are shown in Fig. 23. The form, waviness and roughness components are combined by modes $\{f_i(x,y)|i = 1, 2, \dots, 162\}$, $\{f_i(x,y)|i = 163, 164, \dots, 857\}$ and $\{f_i(x,y)|i = 858, 859, \dots, 1600\}$ respectively. Furthermore, the waviness and roughness parameters are calculated and the result is shown in Table 9. The measurement comparison results of roughness are shown in Table 10. The result shows that all of the parameters are in-of-tolerance. Hence, it can infer that the pump spool bore surface is standard and the manufacture process is stable.

5.3. Case study III

The last case is an aluminum alloy made engine cylinder head surface and a Cast iron FC250 made block surface with multiple holes. The two dimensional diagrams are shown in Fig. 24. The geometrical specification standard of engine cylinder head as $R_a = 3.2\mu\text{m}$ and $R_z = 12.5\mu\text{m}$ are adopted, and the cutoff wavelengths are $\lambda_s = 0.008\text{mm}$, $\lambda_c = 2.5\text{mm}$ and $\lambda_f = 8\text{mm}$ respectively. The roughness standard of the block surface are $R_a = 1.6\mu\text{m}$ and $R_z = 6.3\mu\text{m}$, and the cutoff wavelengths are $\lambda_s = 0.0025\text{mm}$, $\lambda_c = 0.8\text{mm}$ and $\lambda_f = 2.5\text{mm}$ respectively. Four random areas (continuous area C_1 and D_1, discontinuous area C_2 and D_2 shown in Fig. 24) are selected for analysis. The original surfaces are shown in Fig. 25. The modal coordinates and the wavelengths of the four surfaces are depicted in Fig. 26. For surface C_1, the form, waviness and roughness components are combined by modes $\{f_i(x,y)|i = 1, 2, \dots, 28\}$, $\{f_i(x,y)|i = 29, 30, \dots, 400\}$ and $\{f_i(x,y)|i = 401, 402, \dots, 1000\}$ respectively (see Fig. 27). For surface C_2, the form, waviness and roughness components are combined by modes $\{f_i(x,y)|i = 1, 2, \dots, 35\}$, $\{f_i(x,y)|i = 36, 37, \dots, 378\}$ and $\{f_i(x,y)|i = 379, 380, \dots, 1400\}$ respectively (see Fig. 28). For surface D_1, the form, waviness and roughness components are combined by modes $\{f_i(x,y)|i = 1, 2, \dots, 53\}$, $\{f_i(x,y)|i = 54, 55, \dots, 985\}$ and $\{f_i(x,y)|i = 986, 987, \dots, 1500\}$ respectively (see

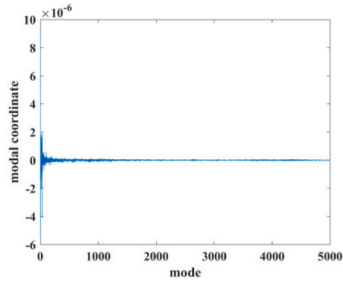


Modal coordinates

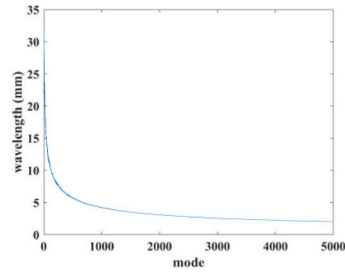


Wavelengths

(a)

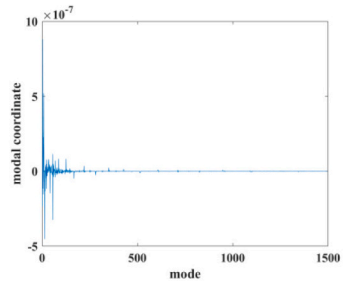


Modal coordinates

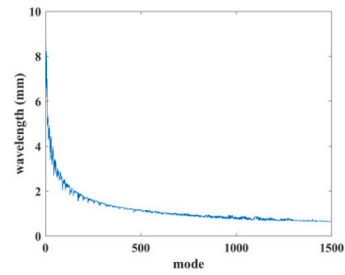


Wavelengths

(b)

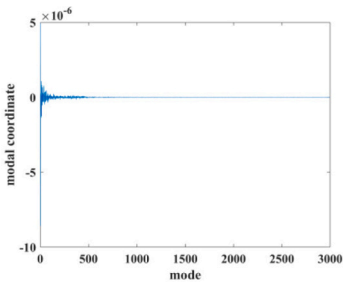


Modal coordinates

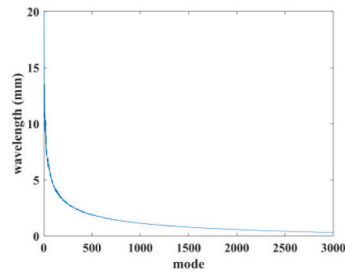


Wavelengths

(c)



Modal coordinates



Wavelengths

(d)

Fig. 26. The modal coordinates and the wavelengths (a) surface C_1 (b) surface C_2 (c) surface D_1 (d) surface D_2.

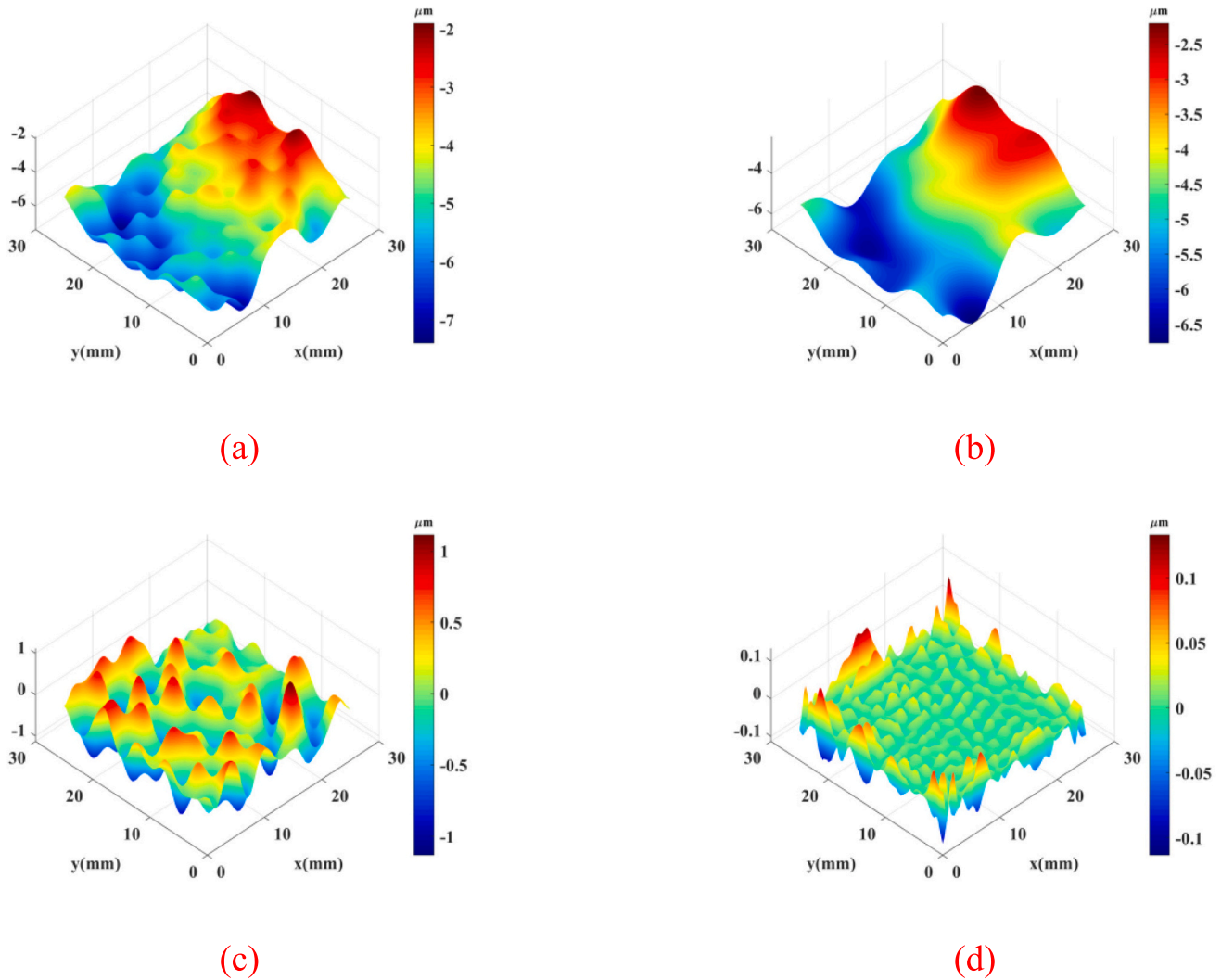


Fig. 27. The filtering results of C_1 (a) the surface reconstructed by first 2000 modes (b) form component (c) waviness component (d) roughness component.

Fig. 29). For surface *D_2*, the form, waviness and roughness components are combined by modes $\{f_i(x,y)|i = 1,2,\dots,223\}$, $\{f_i(x,y)|i = 224,225,\dots,1513\}$ and $\{f_i(x,y)|i = 1514,1515,\dots,3000\}$ respectively (see Fig. 30). Likewise, the waviness and roughness parameters are calculated which shown in Table 11. The measurement comparison results of roughness are shown in Table 12, and the differences between the EDMD filtered values and the measured values are very small which can be ignored. It is clearly that the areal surface parameters of the four surfaces are both in-of-size, which illustrates that the surface quality of the engine cylinder head and the block meet the tolerance standards and the machining process is stable.

6. Conclusions

This research presents a novel surface filtering method named extended discrete modal decomposition (EDMD), which consists of data transforming, surface inverse modeling, extended discrete modal decomposition and quantitative evaluation. The main improved aspects of the EDMD method are list as follows:

- (1) The proposed EDMD method is a nonlinear and non-stationary filtering method, which overcomes the end effect when analyzing the engineering surface topography especially for discontinuous surfaces with holes.
- (2) The physical dimension of the specific mode is complemented, which is an extension of the original DMD.
- (3) The corresponding mapping relationship between discrete modes and surface components is built.

For purpose of verifying the performance and validity of the proposed EDMD method, Gaussian filter, Cutoff Gaussian filter, robust Gaussian regression filter, spline filter, extended tetrolet transform and EDMD method are applied to the same simulated surfaces for visualization and quantitative comparison. Both of simulation studies and case studies can indicate that the proposed EDMD method is feasible and applicable. Moreover, areal surface parameters are used for quantitative evaluation and the results can judge the machining quality and whether the functional behavior of the product has been changed. Hence, the proposed EDMD method provides a new idea of surface topography filtering and can be an available tool in surface analysis.

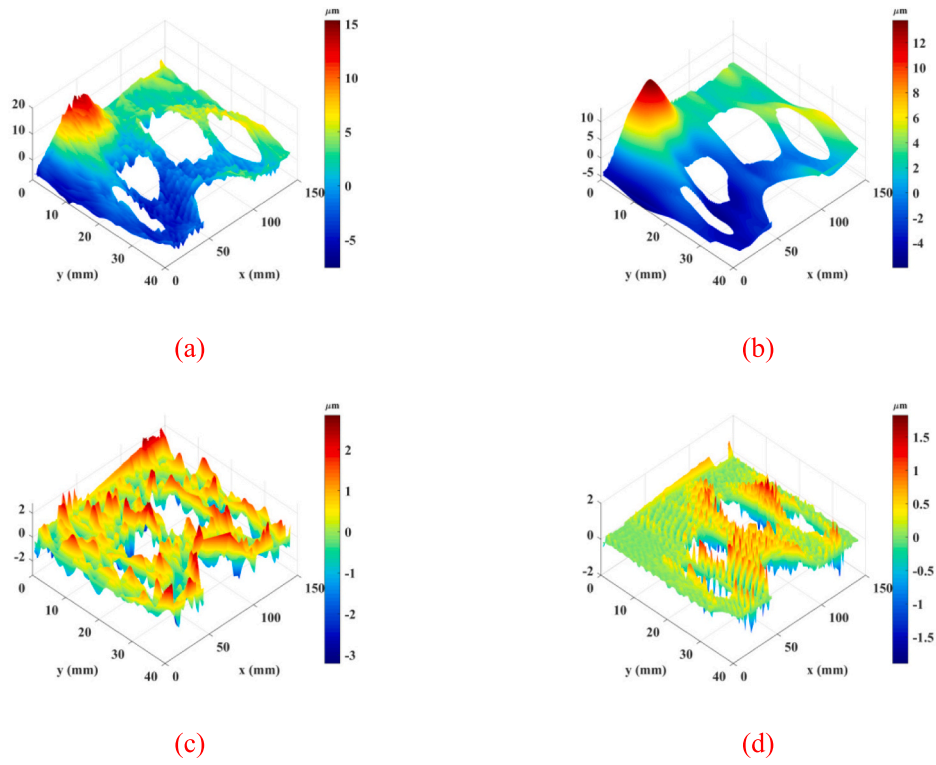


Fig. 28. The filtering results of C_2 (a) the surface reconstructed by first 5000 modes (b) form component (c) waviness component (d) roughness component.

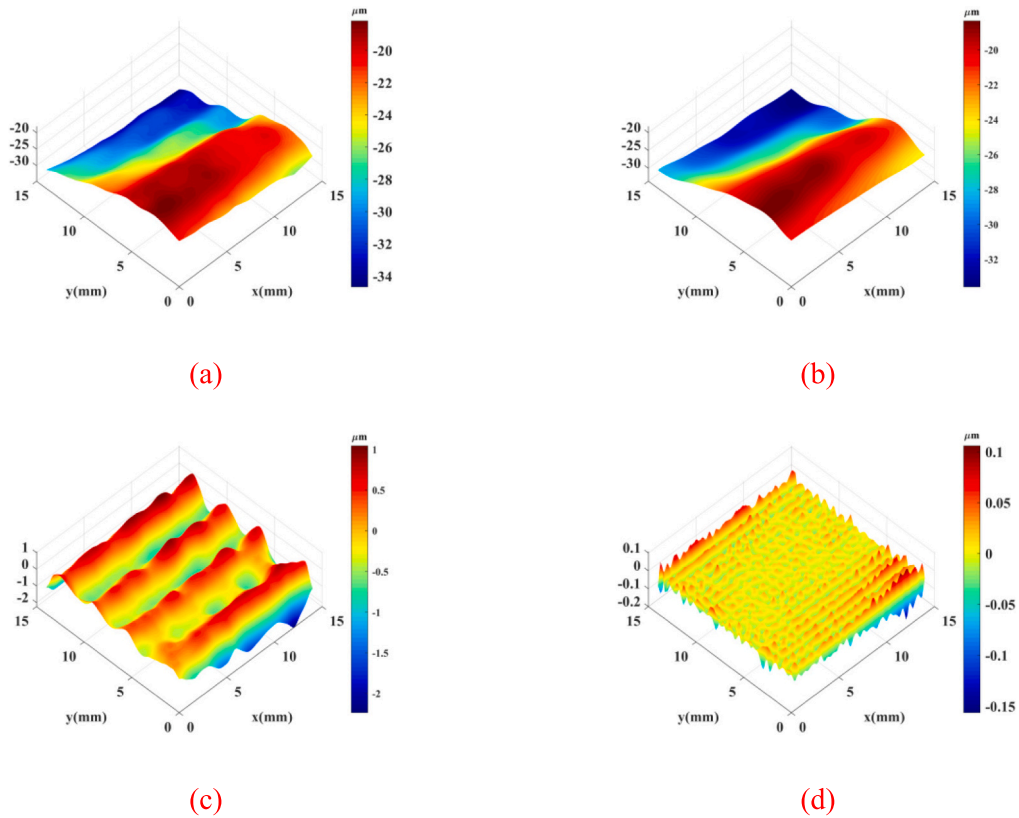


Fig. 29. The filtering result of D_1 (a) the surface reconstructed by the first 1500 modes (b) form component (c) waviness component (d) roughness component.

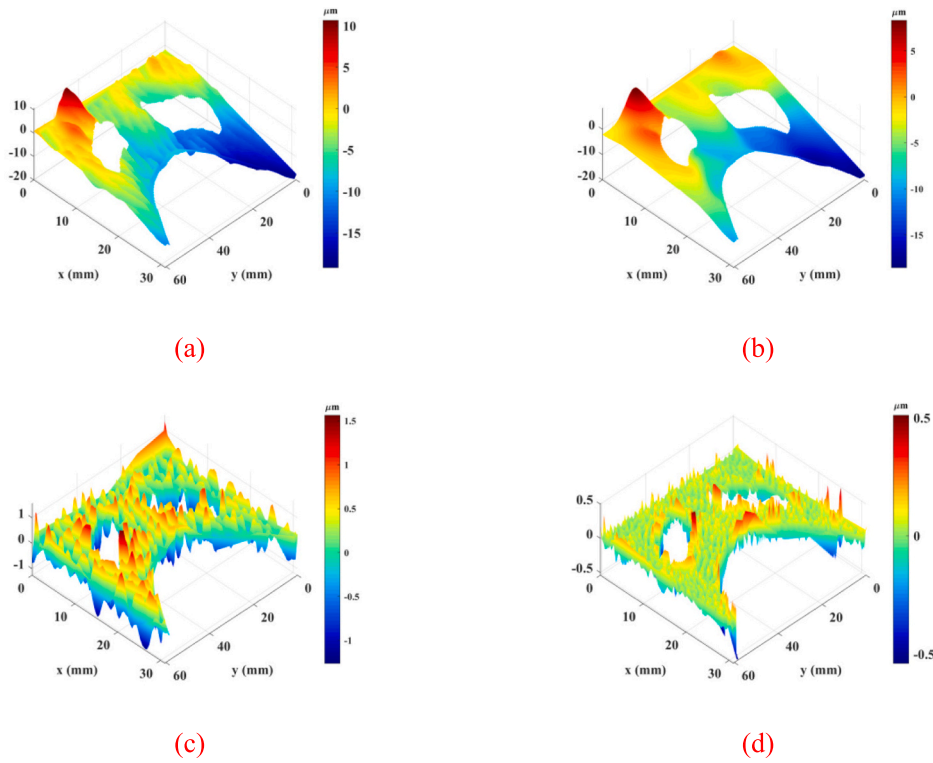


Fig. 30. The filtering results of D_2 (a) the surface reconstructed by the first 3000 modes (b) form component (c) waviness component (d) roughness component.

Table 11
Quantitative evaluations for waviness and roughness components.

Unit (mm)	S_q	S_{sk}	S_{ku}	S_z	S_p	S_v	S_a	S_{dq}	S_{dr}	S_k
C_1_Waviness	0.359	-0.050	2.866	2.258	1.114	1.144	0.283	0.312	0.013	0.363
C_1_Roughness	0.022	0.400	9.110	0.246	0.131	0.116	0.014	0.315	0.015	0.013
C_2_Waviness	0.744	0.180	3.724	6.249	3.088	3.161	0.576	0.411	0.021	0.742
C_2_Roughness	0.376	0.016	5.142	3.898	1.950	1.948	0.259	0.405	0.017	0.228
D_1_Waviness	0.492	-0.634	3.565	3.240	1.026	2.214	0.396	0.336	0.030	0.621
D_1_Roughness	0.032	-0.202	4.232	0.280	0.118	0.163	0.024	0.341	0.032	0.030
D_2_Waviness	0.426	0.336	2.654	2.851	1.566	1.284	0.346	0.511	0.046	0.419
D_2_Roughness	0.075	-0.129	7.293	1.119	0.556	0.563	0.054	0.527	0.053	0.064

Table 12
The measurement comparison results of roughness.

Unit (mm)	R_q	R_{sk}	R_{ku}	R_z	R_p	R_v	R_a
C_1	0.026	0.386	9.024	0.258	0.146	0.112	0.016 ^a
C_2	0.368	0.023	5.137	3.881	1.972	1.909	0.247
D_1	0.038	-0.210	4.229	0.271	0.122	0.149	0.029
D_2	0.081	-0.133	7.289	1.126	0.548	0.578	0.056
D_C_1	-0.004	0.014	0.086	-0.012	-0.015	0.004	-0.002
D_C_2	0.008	-0.007	0.005	0.017	-0.022	0.039	0.012
D_D_1	-0.006	0.008	0.003	0.009	-0.004	0.014	-0.005
D_D_2	-0.006	0.004	0.004	-0.007	0.008	-0.015	-0.002

^a D_C_1 is calculated as (C_1_Roughness - C_1), D_C_2 is calculated as (C_2_Roughness - C_2), D_D_1 is calculated as (D_1_Roughness - D_1) and D_D_2 is calculated as (D_2_Roughness - D_2).

With the development of production requirements, the current product and its surface shape become more complex including continuous and discontinuous structured surfaces, unstructured surfaces and multi-hole freeform surfaces in advanced manufacturing equipment. These surfaces belong non-Euclidean surfaces, and their Gaussian curvatures are not zero and various, which leads to the failed work of the traditional filtering method. Hence, to further enhance the EDMD method or investigate a new filtering method for non-Euclidean surfaces is the next research direction.

Declaration of competing interest

The authors declare that they have no known competing financial interests or personal relationships that could have appeared to influence the work reported in this paper.

Acknowledgements

This work is supported by Natural Science Foundation of Zhejiang

Province (Grant No. LQ22E050017), Zhejiang Science and Technology Plan Project (Grant No. 2018C01003), Postdoctoral Science Foundation of China (Grant No. 2021M702894) and Zhejiang Provincial Postdoctoral Science Foundation (Grant No. ZJ2021119).

References

- [1] Ramasamy SK, Raja J. Performance evaluation of multi-scale data fusion methods for surface metrology domain. *J Manuf Syst* 2013;32:514–22.
- [2] Feng JL, Sun ZL, Jiang ZH, Yang L. Identification of chatter in milling of ti-6Al-4V titanium alloy thin-walled workpieces based on cutting force signals and surface topography. *Int J Adv Manuf Technol* 2016;82:1909–20.
- [3] Yin YX, Shao YP, Wang K, Du SC, Xi LF. Segmentation of workpiece surfaces with tool marks based on high definition metrology. *J Manuf Process* 2020;57:268–87.
- [4] Ledoux Y, Lasseux D, Favreliere H, Samper S, Grandjean J. On the dependence of static flat seal efficiency to surface defects. *Int J Press Vessel Pip* 2011;88:518–29.
- [5] Liao Y, Stephenson DA, Ni J. A multifeature approach to tool wear estimation using 3D workpiece surface texture parameters. *J Manuf Sci E T ASME* 2010:132.
- [6] Liu NC, Liu BL, Jiang H, Wu SH, Yang CW, Chen Y. Study on vibration and surface roughness in MQCL turning of stainless steel. *J Manuf Process* 2021;65:343–53.
- [7] Malburg MC. Surface profile analysis for conformable interfaces. *J Manuf Sci E T ASME* 2003;125:624–7.
- [8] Nguyen HT, Wang H, Hu SJ. Characterization of cutting force induced surface shape variation in face milling using high-definition metrology. *J Manuf Sci E T ASME* 2013:135.
- [9] Yin YX, Du SC, Shao YP, Wang K, Xi LF. Sealing analysis of face-milled surfaces based on high definition metrology. *Precis Eng* 2022;73:23–39.
- [10] Lorenz B, Persson BNJ. On the dependence of the leak rate of seals on the skewness of the surface height probability distribution. *Epl* 2010:90.
- [11] Brown CA, Hansen HN, Jiang XJ, Blateyron F, Berglund J, Senin N, et al. Multiscale analyses and characterizations of surface topographies. *CIRP Ann Manuf Technol* 2018;67:839–62.
- [12] Raja J, Muralikrishnan B, Fu S. Recent advances in separation of roughness, waviness and form. *Precis Eng* 2002;26:222–35.
- [13] ISO 16610-61. Geometrical Product Specifications (GPS)-Filtration Part 61, linear areal filters: Gaussian filters. 2010.
- [14] Brinkmann S, Bodschiwinna H, Lemke HW. Accessing roughness in three-dimensions using Gaussian regression filtering. *Int J Mach Tools Manuf* 2001;41:2153–61.
- [15] Brinkman S, Bodschiwinna H. Advanced Gaussian filters - advanced techniques for assessment surface topography - 4: advanced gaussian filters - advanced techniques for assessment surface topography - 4. 2003.
- [16] Seewig J. Linear and robust Gaussian regression filters. In: 7th symposium on measurement technology and intelligent instruments. Huddersfield, ENGLAND: Univ Huddersfield; 2005. p. 254–7.
- [17] Janecki D. Edge effect elimination in the recursive implementation of gaussian filters. *Precis Eng* 2012;36:128–36.
- [18] Whitehouse DJ. Theoretical enhancement of the gaussian filtering of engineering surfaces. *P Roy Soc A-Math Phys* 2013:469.
- [19] Kondo Y, Numada M, Yoshida I, Yamaguchi Y, Machida H, Koshimizu H. Robust filter compatible with gaussian filter using L2-norm. *Precis Eng* 2022;76:124–32.
- [20] Krystek M. Form filtering by splines. *Measurement* 1996;18:9–15.
- [21] Krystek M. Transfer functions of discrete spline filters. In: *Advanced Mathematical Tools in Metrology III*; 1997. p. 203–10.
- [22] Jiang XQ, Blunt L, Stout KJ. Development of a lifting wavelet representation for surface characterization. *Proc Math Phys Eng Sci* 2000;456:2283–313.
- [23] Fu SY, Muralikrishnan B, Raja J. Engineering surface analysis with different wavelet bases. *J Manuf Sci E-T ASME* 2003;125:844–52.
- [24] Huang NE, Shen Z, Long SR, Wu MLC, Shih HH, Zheng QN, et al. The empirical mode decomposition and the Hilbert spectrum for nonlinear and non-stationary time series analysis. *P Roy Soc A-Math Phys* 1998;454:903–95.
- [25] Du SC, Liu CP, Huang DL. A shearlet-based separation method of 3D engineering surface using high definition metrology. *Precis Eng* 2015;40:55–73.
- [26] Du SC, Liu T, Huang DL, Li GL. A fast and adaptive bi-dimensional empirical mode decomposition approach for filtering of workpiece surfaces using high definition metrology. *J Manuf Syst* 2018;46:247–63.
- [27] Shao Y, Du S, Tang H. An extended bi-dimensional empirical wavelet transform based filtering approach for engineering surface separation using high definition metrology. *Measurement* 2021;178.
- [28] Shao Y, Wang K, Du S, Xi L. High definition metrology enabled three dimensional discontinuous surface filtering by extended tetrolet transform. *J Manuf Syst* 2018;49:75–92.
- [29] Jiang XQ, Lou S, Scott PJ. Morphological method for surface metrology and dimensional metrology based on the alpha shape. *Meas Sci Technol* 2012;23.
- [30] Lou S, Jiang X, Scott PJ. Application of the morphological alpha shape method to the extraction of topographical features from engineering surfaces. *Measurement* 2013;46:1002–8.
- [31] Lou S, Pagani L, Zeng W, Jiang X, Scott PJ. Watershed segmentation of topographical features on freeform surfaces and its application to additively manufactured surfaces. *Precis Eng* 2020;63:177–86.
- [32] Samper S, Formosa F. Form defects tolerancing by natural modes analysis. *J Comput Inf Sci Eng* 2007;7:44–51.
- [33] Le Goic G, Favreliere H, Samper S, Formosa F. Multi scale modal decomposition of primary form, waviness and roughness of surfaces. *Scanning* 2011;33:332–41.
- [34] Pitard G, Le Goic G, Mansouri A, Favreliere H, Desage SF, Samper S, et al. Discrete modal decomposition: a new approach for the reflectance modeling and rendering of real surfaces. *Mach Vision Appl* 2017;28:607–21.
- [35] Wu ZH, Huang NE. A study of the characteristics of white noise using the empirical mode decomposition method. *P Roy Soc A-Math Phys* 2004;460:1597–611.
- [36] ISO 4287. Geometrical product specifications (GPS)-Surface texture: profile method: terms, definitions and surface texture parameters. 1997.
- [37] Felsberg M, Sommer G. The monogenic signal. *IEEE Trans Signal Process* 2001;49:3136–44.
- [38] ISO 25178-2. Geometrical product specifications(GPS)-Surface texture: Areal - Part 2: Terms, definitions and surface texture parameters. 2012.
- [39] ISO 25178-3. Geometrical product specifications (GPS) — surface texture: areal — part 3: specification operators. 2012.